Diurnal cycle of coastal anthropogenic pollutant transport over southern West Africa during the DACCIWA campaign

Adrien Deroubaix, Laurent Menut, Cyrille Flamant, Joel Brito, Cyrielle Denjean, Volker Dreiling, Andreas Fink, Corinne Jambert, Norbert Kalthoff, Peter Knippertz, Russ Ladkin, Sylvain Mailler, Marlon Maranan, Federica Pacifico, Bruno Piguet, Guillaume Siour, Solène Turquety

Dear Editor,

We thank you and the referees for their reports. We propose in the following answers along with the appropriate corrections of the manuscript.

1 Report 1

1.1 General Description

The authors use surface and aircraft observations, radiosondes, satellite observations, and a model to determine the diurnal cycles of NOx and CO at a short-term monitoring site in southern West Africa and assess the contribution of individual sources and synoptic-scale meteorology to this diurnal variability. The figures are clearly presented and the model tracer simulation experiment is informative of the varying contribution of pollution from cities and other sources to pollution at the monitoring site. The content is appropriate for ACP, but there is limited context for the relevance of the results for other time periods and locations in southern West Africa and the implications of findings for future air quality due to increasing urbanisation and changes in biomass burning (Andela et al., 2014). It is for this reason that I'm hesitant to accept as is and highly recommend that the authors strengthen the relevance of the paper by addressing its limited scope.

We acknowledge the reviewer for her/his constructive comments. About the relevance of the paper for other locations or other time periods, we added sentences to state more precisely this important point. The following sentence was added at the end of the introduction, p.3 l.23: *'This study is focused on one specific period and location. However, the conclusions are representative of a longer time period as meteorological conditions at the coast during the so-called monsoon post-onset period were found to be quite stable for several weeks (Knippertz et al., 2017). Spatially, the results are directly representative of the studied region only, the main goal being to estimate the influence of the emissions from four coastal cities on the atmospheric composition in the lower troposphere over inland Benin. Given the broad southwesterly monsoon flow in the region, a similar transport from coastal pollution inland will likely be found along the most of the Guinea Coast.'*

1.2 General Comments

- How does the paper fit within the context of other findings from analysing observations and model output during DACCIWA, and also enhance understanding of the region since the AMMA campaign?

  The main goals of the two projects are rather different. In the introduction, we have added the sentence: *'AMMA was focused on the Sahelian region combining a multi-scale approach to better characterize the interactions between atmosphere, land and ocean during the monsoon (Janicot et al., 2008; Redelsperger et al., 2006), whereas the DACCIWA project is dedicated to the interactions between aerosols, clouds and radiation along the highly urbanized coastline of the Gulf of Guinea (Knippertz et al., 2015).'*.
  In this context, this paper aims at focusing on the transport of pollutants from coastal cities to a remote inland site. We have shown that there is a specific time of the day (16:00 to 03:00 UTC) for the transport of pollutants from the coast to the north, which is in agreement with observations and other modeling studies by Adler et al. (2017) and Deetz et al. (2018).

- There are many typos that can be eliminated with a careful reread (extents on P2, L5; 21th on P2, L9; acquiered on P4, L18 etc.).

  The new manuscript has been carefully checked and corrected.

- Please fix incorrect order of in-text citations when there is more than one article in the same year by the same first author (P2, L14; P2, L27 etc.).

  The citations are automatically managed by Latex/bibtex package of the Journal. It has been fixed in the new version and it will have to be control at the proof stage.

- Why does the study focus on Savè, beyond logistics? Is there rapid population increase? Is it an ideal location to understand synoptic scale meteorological patterns in southern West Africa? This could be better justified.

  The study focuses on Savè for two reasons: this is one of the three super-site of the DACCIWA project, and it is the most suited of the three sites to analyze the pollution transport from coast to inland areas because of the low local emissions. As a super-site, a lot of original measurements have been made of air quality issues often affecting smaller inland cities during the campaign. This site is representative of inland air quality, often under the plume of coastal cities.
  This was reworded in the Introduction: the sentence: *'The super-site of Savè serves as a representative location of inland air quality.'* has been modified to: *'The super-site of Savè is a representative location to assess the impact of pollution transport from the coast on the air quality of remote inland cities characterized by low local emissions.'*
  In Section 2.2 (part Ground based station) a paragraph has been added: *'Three super-sites have been implemented in the framework of the DACCIWA project in Kumasi (Ghana), Ile-Ife (Nigeria) and Savè (Benin). Unlike the two others, Savè is representative of transport-related air quality issues affecting small cities, characterized by low local emissions, downstream of large coastal cities. It is ideal in that the terrain is very flat with no orographically induced circulation impacting the monsoonal flow. Thus to study NOx and CO from coastal urbanized areas, this rural environment is well suited.'*
  Moreover, in the Conclusions, a sentence has been added: *'We analyzed pollution transport from the main urban emission centres of the Guinea Coast (Abidjan, Accra, Lomé, Cotonou and Lagos) at the super-site of Savè in order to assess the impact on the air quality of remote inland cities characterized by low local emissions.'*

- Only 7 days of observations are considered. Can we draw conclusions about an extended time period based on this brief analysis period? And if so, what time period? The full year? The entire monsoon period? The onset period only?

  Of course, knowing the meteorology in this region, the study is not representative of the whole year. These 7 days are representative of a longer period, mostly the post-onset period defined from 22 June to 20 July by Knippertz et al. (2017). The monsoon flow was not very variable during this period, at least not in direction, as it has been shown by Kalthoff et al. (2018). Moreover, there is a case of long-range transport of biomass burning aerosol from Central Africa during these seven days (Flamant et al., 2018b). This is now better explained in the introduction with the addition of the sentence: *'These seven days are representative the onset period defined from 22 June to 20 July by Knippertz et al. (2017) because of the quite stable wind conditions(Kalthoff et al., 2018). '*

- Absent from the study are measurements and/or a discussion of non-methane volatile organic compounds (NMVOCs) and aerosol mass concentrations and composition. Emissions of these are high from local sources and from distant biomass burning (Liousse et al., 2014; Marais et al., 2016; Janicot et al., 2008; Reeves et al., 2010). Can the same conclusions about sources and diurnal variability be drawn about these? Were these measurements made during DACCIWA on the aircrafts flown? If so, do these offer any utility in understanding these pollutants or confirming similar diurnal behavior? If not, are there other studies that could be referenced to assess the sources of these pollutants and the implications for air quality?

  The goal of the paper is not to extensively study all chemical compounds. We have selected NO_x and CO for the sake of simplicity. These two species are enough for the topic of the paper: NO_x is representative of anthropogenic emissions, whereas CO is representative of both anthropogenic and fires emissions. Of course, the addition of VOC and aerosol compositions could be very interesting, but it could blur our message, more focused on meteorology and transport. The chemical concentrations presented in this paper are used to demonstrate that there is a clear pollution transport diurnal cycle associated with each of the four coastal cities on the remote site of Savè.

- Change MODIS-AOD to MODIS AOD throughout.

  This has been changed.

- The figures are presented out of sequence in the text (e.g. Figures 11 and 12 are mentioned before Figure 3). Please reorder the figures so that these are introduced sequentially.

  This is corrected in the new version. It is a problem coming from the compatibility between different Latex's packages.

- Include a link to the MODIS AOD product used in this work (preferably doi, otherwise URL).

  DOIs have been included in the new version.

- Shorten the conclusion to the main findings of the paper, rather than providing a detailed overview of the methods, results, and outcomes.

  The conclusion was rewritten to focus on the main results only.

1.3 Specific Comments

- P3, L12: Consider instead referencing a relevant publication from AMMA or from analysis of MOZAIC vertical profiles that finds influence of Central African biomass burning on atmospheric composition in southern West Africa.

  The citation of an article in preparation has been changed to Reeves et al. (2010).

- Table 1: The table title says 2015 population but from a 2011 Revision. Are these projected estimates? Why not use a recent revision? No reference is provided for the 2011 Revision, so it's not possible to assess what the 2015 population is when it was revised in 2011.

  The reference and the url have been included in the new version as a citation (United Nations report, 2011).

- Section 2.2: Are the dashed indented lines headers? These are unnecessary. Instead integrate these in the relevant paragraph and make clear in the first sentence what the paragraph is about.

  We have followed the reviewer' suggestion.

- P5, L9: How frequently are the radiosondes launched during the time period considered in this study?

  In Savè, radiosondes were launched every 1.5 to 3 hours. It has been added in the new version.

- P5, L12-17: How are biomass burning layers identified with a total column AOD measurement?

  The reviewer is right, it is not possible to characterize aerosol vertical layers with an AOD product. The sentence *'We analyze the spatial extent of BB layers from satellite observations'* has been changed to *'We analyze the horizontal spatial extent of the main aerosol plumes from satellite observations'*.

- P5, L20: How accurate is CALIOP at distinguishing aerosol types?

  As in the case of this study, when remotely sensed aerosols have very different optical properties (dust, biomass burning, sea salt), the CALIOP aerosol classification is robust. This is more thoroughly discussed in the following publication (also made in our team): *Menut, L., Flamant, C., Turquety, S., Deroubaix, A., Chazette, P., and Meynadier, R.: Impact of biomass burning on pollutant surface concentrations in megacities of the Gulf of Guinea , Atmos. Chem. Phys., 18, 2687-2707, https://doi.org/10.5194/acp-18-2687-2018, 2018.* This reference and an explanation was added in the Section 2.2: *'In order to identify the altitude of aerosols together with their speciation, we use the space-borne Cloud-Aerosol Lidar with Orthogonal Polarization (CALIOP) aerosol type classification (Winker et al., 2009). This classification is suited and accurate to distinguish homogenous aerosol plumes with different optical properties such as sea salt, dust and BB (e.g. Menut et al., 2018).'*.

- P5, L28-29: Knippertz et al. (2017) isn't the seminal paper on defining the monsoon onset period. Do the authors mean to say that the monsoon onset period specific to DACCIWA (2016) is 22 June to 20 July?

  This article deals only with the 2016 WAM. Our studied period is the post-onset period for the WAM 2016. This is now specified in Section 2.3: *'The studied period (1 to 7 July) is entirely included in the 2016 WAM post-onset phase, which has been defined from 22 June to 20 July 2016 by Knippertz et al. (2017).'.*

- P6, L23-30: Elaborate on the pseudo-anthropogenic emissions that are imposed. Are these based on an existing inventory? How much is emitted per one million inhabitants? Does the imposed magnitude of emissions matter?

  The expression *'pseudo-anthropogenic emissions'* is misleading. We want to scale the tracer emissions to the size of the agglomeration (Section 2.1), as it has been done by Flamant et al. (2018a). This paragraph has been reworded: *'In this study, the model is used in its tracer version and there is no atmospheric chemistry. We choose to release passive gaseous tracers in the simulation, because we want to analyze only their transport (no chemistry, no deposition) caused by the monsoonal flow. Since we want to distinguish the relative contribution of several coastal cities to the pollution further inland, we designed a first experiment for which we impose the tracer emissions at specific urbanized locations: Abidjan (Ivory Coast), Accra (Ghana), Lomé (Togo), Cotonou (Benin), Lagos (Nigeria) (cf. Table 1 for coordinates). Specific tracers are emitted for a given city in order to distinguish their relative contributions at inland locations. Thus the tracer emissions occur in a single grid cell corresponding to the center of each city.'*

- P7, L9-11: Was there any rain during 1-7 July that would cause aerosols to wet deposit and so affect interpretation of output from a model that does not include sinks?

  The following sentence has been included in Section 2.3.2: *'The period is not associated with widespread rain. At Savè, there were only some small precipitation events (Kalthoff et al., 2018). We focus our analysis on gaseous species but we suppose similar transport patterns for aerosol and gaseous pollutants because of the constant monsoon flow blowing over SWA during our studied period.'*

- P7, L26-28: This transport pattern has already been observed during AMMA and before that using MOZAIC aircraft campaign observations. Consider including these studies too to reinforce that this work builds on previous research and campaigns.

  We have included two articles from the AMMA campaign results. These sentences have been modified: *'The origin of the high AOD over the Gulf of Guinea is well known. This is the BB layer coming from Central Africa, where intense vegetation fires occur during this season (Giglio et al., 2006) with increasing trends over the period 2001-2012 (Andela and Van Der Werf, 2014). Part of this pollution is transported over the Gulf of Guinea and the BB plume reaches the Guinea Coast was seen during the AMMA campaign (Sauvage et al., 2005; Reeves et al., 2010). The BB pollutant concentrations observed along the Guinea Coast depend on the synoptic wind patterns (Menut et al., 2018). '*

- Figure 3: How representative is the site of the coincident 2 km x 2 km model gridsquare?

  In the legend of Figure 3, we have added the sentence: *'WRF-derived variables are interpolated to the radiosonde positions'.*

- Section 3.2: 'From research aircraft' and 'From radiosondes' are not complete headers. Consider revising.

  The titles have been revised as follows: Section 3.2 *'Vertical layers in the lowermost troposphere'*; and Subsections 3.2.1 *'Identification from radiosondes'* as well as 3.2.2 *'Identification from research aircraft'.*

- P11, L1: Why define this "feature G". It's not used again and doesn't seem to appear in any of the figures.

  This was unclear and unnecessary. 'Feature G' refers to a feature described in Knippertz et al. (2017). The parenthesis *'(described as feature G in this study)'* has been removed.

- P12, L30-35: Does interference in the NO2 measurement from dissociation of NOx reservoir compounds (Reed et al., 2016) impact the interpretation of NO2 and NO2/NO diurnal variability?

  The interference described in Reed et al. (2016) is significant for low NO_x concentration (about 10 ppt). Given the relatively high concentrations of NO_x (greater than 0.2 ppb) over our domain, we can assume a low effect of this process on our results.

- P13, L27-29: This result isn't surprising, as the monsoon flow is prevailing southwesterly and so transport from Lagos isn't expected. It would be more noteworthy if this did occur.

  We agree with the reviewer. The sentence *' It is worthy of note that Lagos tracers do not reach Savè, although emissions from Lagos are greater than from the other cities.'* has been replaced by *'Lagos tracers do not reach Savè because of the southwesterly monsoon flow.'*.

- P14, L1: What is the implication on future air quality that the Cotonou plume affects Savé?

  The anthropogenic emissions of the agglomeration of Cotonou are supposed to rise because the population is quickly growing. Beyond this point, our results have shown that there is a specific time of the day (16:00 to 02:00 UTC) for the transport of pollutants from the coast toward the north. There are implications for inland air quality over SWA, human health as well as radiative transfer and the diurnal cycle of low-level clouds.
  We have added a sentence in the Conclusions: *'There is a specific time of the day (16:00 to 02:00 UTC) for the transport of pollutants from the coast toward the north, which affects inland air quality over SWA, human health as well as radiative transfer and low-level cloud diurnal aspects.'*

- Videos: Consider adding annotations or narration to the videos to guide the viewer. Also consider adding time stamps in the text to point the reader to these specific features in the videos.

  We have followed the reviewer suggestion by adding time stamps in the text of Section 4.3: *'From the wind patterns, we note that the coastal front is present from 09:00 to 15:00 UTC from the coast up to ≈ 7°N. It leads to the accumulation of URB pollutants. This period is referred to 'Daytime drying' by Deetz et al. (2018). From 16:00 to 02:00 UTC (respectively from 03:00 to 08:00 UTC), the meridional wind increases (resp. decreases) in the PBL and URB pollutants are mostly transported northward within the PBL. This period is referred to 'Atlantic inflow' (resp. 'Moist morning') by Deetz et al. (2018).*
  During the 'Daytime drying' period, we notice that URB and BB tracers accumulate along the coastline in the PBL (on 5 and 6 July from 11:00 to 15:00 UTC). When dry convection stops (at 16:00 UTC), wind speed quickly increases with a stronger northward component. BB and URB tracers are simultaneously transported northward from the coast. From 16:00 to 02:00 UTC, the front moves towards the north, and the mixture of BB and URB tracers is advected accordingly. A similar diurnal evolution of BB and URB transport is simulated on 5 and 6 July. '

1.4 References

- Andela et al., doi:10.1038/nclimate2313, 2014.
- Janicot et al., doi:10.5194/angeo-26-2569-2008, 2008.
- Knippertz et al., doi:10.5194/acp-17-10893-2017, 2017.
- Liousse et al., doi:10.1088/1748-9326/9/3/035003, 2014.
- Marais et al., doi:10.1021/acs.est.6b02602, 2016.
- Reed et al., doi:10.5194/acp-16-4707-2016, 2016.
- Reeves et al., doi:10.5194/acp-10-7575-2010, 2010.

All these references are now included; except Reed et al. (2016) because the interference described in this article is significant for low NO_x concentration (about 10 ppt).

2 Report 2

2.1 General Description

The authors used ground-based and aircraft measurements of meteorological and chemical (CO, NO, NO2) variables collected during DACCIWA campaign to understand the transport pathway of biomass burning and coastal urban emissions in SWA. To further investigate this, they designed and used two experiments using WRF-CHIMERE (in tracer mode). First, they thoroughly studied the model performance and its limitations in capturing the transport. Next, they used the tracer experiments to assess the contribution of urban and biomass burning pollutions in the region. The manuscript is well written, and I recommend it for ACP after fixing the typos and addressing some issues listed below.

We thank the reviewer for her/his positive comments.

2.2 General Comments

- There are mistakes in the order of references and format of the references in the introduction. Please double check the references.

  It has been entirely revised.

- UTC and local time description (morning/evening) were used interchangeably. Please provide information on the time zone and sunset/sunrise time.

  This information have been added in Section 2.2: *'Our studied domain is located in the Greenwich Mean Time (GMT). Hence local time is the same as UTC. During the aircraft campaign period, sunrise occurred arund 06:00 UTC and sunset around 18:00 UTC.'*

- The section on population can be shortened as some parts in introduction and 2.1 overlaps.

  The section 2.1 has been reworded following the other reviewer's comment.

- How does the result compare with the AMMA campaign?

  During the AMMA aircraft campaign, most aircraft operations took place over the Sahel, whereas the DACCIWA aircraft campaign was focused on the Guinea Coast. Moreover, the goal of the AMMA project was to better characterize the interactions between atmosphere, land and ocean during the monsoon (Janicot et al., 2008; Redelsperger et al., 2006), whereas the DACCIWA project was dedicated to the interactions between aerosols, clouds and radiation along the highly urbanized coastline of the Guinea Coast (Knippertz et al., 2017).
  In the introduction, we have added the sentence: *'AMMA was focused on the Sahelian region combining a multi-scale approach to better characterize the interactions between atmosphere, land and ocean during the monsoon (Janicot et al., 2008; Redelsperger et al., 2006), whereas the DACCIWA project is dedicated to the interactions between aerosols, clouds and radiation along the highly urbanized coastline of the Gulf of Guinea (Knippertz et al., 2017)'.*

- The order of the figures is not correct. Please use supplement material if necessary.

  Supplement material has been added and the order of the figure has been corrected in the new version.

- In section 3.2.2. the discussion on model performance in capturing wind and RH is difficult to follow. Please either discuss layer-by-layer (starting from the lowest layer) or variable by variable.

  We have followed the reviewer's suggestion and this section has been reworded:
  'From the surface to 1 km amsl, the modeled wind speed and direction match well with the observations (absolute bias lower than 0.2 $m.s^{-1}$ and 4^o, respectively). The observed distribution of the monsoon wind is captured by the model up to 1 km amsl (inter-quartile range 3.80 – 6.47 $m.s^{-1}$ for the observations and 3.98 – 6.80 $m.s^{-1}$ in the simulation). The modeled distribution of RH shows a dry bias in the monsoonal flow (of -6 %).
  In the directional shear layer, from 1 to 2 km amsl, observed and modeled wind speed distributions are narrower than in the monsoon layer (inter-quartile ranges being 2.10 – 4.04 $m.s^{-1}$ and 1.88 – 3.94 $m.s^{-1}$ respectively), showing that this layer is well defined over the domain. The modeled wind direction is in good agreement with observations (relative bias lower than 1 %), although with a wider distribution (observed inter-quartile range $191.17 - 285.29^o$ and modeled 214.17 – 237.67^o) than in the first kilometer (observed inter-quartile range 220.08 – 244.41^o and modeled 207.29 – 272.28^o).
  In the main easterly layer, from 2 to 4 km amsl, the observed distribution of wind speed is wider than at lower altitudes, which is in good agreement with the modeled distribution. Observed and modeled RH and

wind direction distributions are also consistent.
In conclusion, during daytime, the monsoon layer is reproduced with a dry bias. The low (relative) biases of wind speed (+4 %) and direction (-2 %) in this layer are of prime importance to accurately model the URB transport.'

- In section 3.2.2. How does the result compare with radiosondes results?

  We use the vertical layers identified with radiosonde observations to analyze the aircraft observations in these layers. Aircraft and radiosondes provide complementary information on horizontal and vertical variability, respectively. It is thus difficult to compare these observations.

- Estimating PBL height from radiosonde measurements (separating day and night measurements) and comparing with model PBL height can be beneficial for the discussion in section 3.3
- I suggest adding more details on the PBL height and its influence on the concentration of different constituent, especially during nighttime.

  We took on the reviewer's comments and started looking into this. However, determining the PBL height from the radiosoundings at the coast proved to be difficult because of the presence of multiple low-level cloud layers as well as the relatively weak associated temperature inversions. The results were not satisfactory, and hence we did not pursue this further. Moreover, Section 3.3 focuses on daytime observations acquired by the aircraft. For the horizontal pollution transport, which is the main concern of the article, our goal is to capture the wind speed and direction. With the numerical tracers, we use an arbitrary unit and no chemistry, thus the dilution volume is not the main driver of the variability.

2.3 Specific Comments

- P3-L1-5: I suggest adding more references on the source attribution to provide a bigger picture. What is the contribution of these sectors in other regions or bigger domains? For example, compare with Sobhani et al., 2018; Yang et al., 2017; Kulkarni et al., 2015

  These references have been added (Kulkarni et al., 2015; Yang et al., 2017; Sobhani et al., 2018) in the introduction as follows: *'In order to better distinguish the contributions from different sources to background concentrations, additional studies are needed focusing on Africa as it has been done for other regions (e.g. Kulkarni et al., 2015; Yang et al., 2017; Sobhani et al., 2018).'*

- P3-L2: What year? 2006?

  Yes, this study was done using datasets acquired during the AMMA campaign in 2006. This sentence has been reworded: *'Using WRF-CHIMERE numerical simulations of the WAM during the African Monsoon Multidisciplinary Analyses (AMMA) campaign period from May to July 2006, Deroubaix et al. (2018) quantified the relative contributions of anthropogenic and biomass burning sources to carbon monoxide (CO) concentrations over SWA, which in July 2006 was about 25 % local anthropogenic and 50 % biomass burning from Central Africa. '*

- P3-L12: "Haslett et al., in preparation" I don't think this is an acceptable format and it is not mentioned in the References section.

  It has been replaced by Reeves et al. (2010).

- P3-L18: "1-7 July" Please add 2016.

  The year 2016 has been added.

- P4-L9: the Lome population stated in the text does not match Table 1.

  We thank the reviewer for picking this up. It has been corrected.

- P4-L10 and the next paragraph: Information given on population of Cotonou is confusing. Is it necessary to state 1,086,00 inhabitant and then change it in the next paragraph?

  With the tracer experiment, we scale the tracer emissions to the size of the population in each city. We have used the estimation of the department of social and economic affairs of United Nations (United Nations report, 2011), except for Cotonou because we were surprised by the fact that Lomé was estimated

bigger than Cotonou. In Section 2.1, we justify this assumption but it was not well written. It has been improved in the new version of the article: *'We focus on six locations, five major urban agglomeration of the Guinean coastal region, and one small town, Savè, which is 185 km north of Cotonou (Benin). Table 1 shows the coordinates and the population of the urban agglomerations studied. For Abidjan, Accra, Lomé and Lagos, we present estimations for the year 2015 of the department of social and economic affairs of United Nations (United Nations report, 2011). In this report, these cities are associated with large administrative areas in contrast to Cotonou.*
Comparing Lomé and Cotonou, Lomé has a large administrative area while Cotonou is a city with a very high population density over a small area. The population of Lomé is about 839,000 inhabitants in the city according to the General Population and Habitat Census of Togo (DGSCN report, 2016) and about 1,830,000 inhabitants in the administrative state (United Nations report, 2011). Cotonou city is estimated by the World Urbanization Prospects report to have about 1,086,000 inhabitants (United Nations report, 2011).
According to the General Population and Habitat Census of Benin (INSAE report, 2015), the population of Cotonou only slightly increased by 2.09 % over the period 2002-2013 because of the limited possibility of expansion. They note that along the shores of Lake Nokou the population has increased rapidly, thus forming an agglomeration of 2,194,000 inhabitants, calculated as the sum of the Cotonou district and several cities of the Atlantique district (Abomey-Calavi and So-Ava) and of the Ouémé district (Seme Kpodji, Porto Novo, Avrankou and Akpro-Misserete). '

- P42-Table 2: Please provide coordinates of the ground sites.

  The ground site coordinates have been provided in Table 2.

- P5-L9: What is the local time?

  In this region and at this time of year, UTC is the same as local time. Following the previous reviewer's comment, indications on time zone have been added in Section 2.2.

- P5-section 2.3: Please add a figure of outer domain.

  The introduction of section 2.3 have been modified to include this information: *'The WRF-CHIMERE simulations presented in this study have a similar set-up to those used by Deroubaix et al. (2018). Both models are run offline in a nested configuration on the same grids with two domains: a regional domain (10 km× 10 km, extending from 1° S to 14° N and from 11° W to 11° E) and a high-resolution coastal domain (2 km× 2 km). The simulations over the regional domain are started on 1 June 2016. In the following, we present only results modeled over the high-resolution domain (Figure 1). The simulated period over the high-resolution domain (1 to 7 July) is entirely included in the 2016 WAM post-onset phase, which has been defined from 22 June to 20 July 2016 by Knippertz et al. (2017). '*.

- P6-L2: How many layers below 1 km?

  This is an important information regarding the goal of our study. It has been added in the introduction of section 2.3.1: *'The domains have a constant horizontal resolution with 32 vertical levels from the surface to 50 hPa, including about 10 vertical levels below 1 km amsl.'*

- P6-L5: Please reference GFS data.

  The DOI is now mentioned: *'Global meteorological fields are taken from the US Global Forecast System (operational final analyses) produced by the National Center for Environmental Prediction (ds083.3 dataset DOI: https://10.5065/D65Q4T4Z)'*

- P6-L5: Did you use GFS data only for nudging or for meteorological initial and boundary conditions as well? Please clarify in the text.

  The GFS dataset has been used for both. It is now clearly stated.

- P6-L14: Did you use cumulus parametrization for both domains?

  The reviewer is right. We use a cumulus parametrization only for the regional domain. This information is now specified in this sentence: *'for the high-resolution domain, convective precipitation is explicitly calculated and not parametrized'*.

- P6-L27: What time do you start releasing the tracers? Have you allowed for spin up in the model before releasing the tracers?

  We use a one month spin-up over the regional domain. This information was missing and has been added in the introduction of Section 2.3: *'The simulation over the regional domain are started on 1 June.'*

- P6-L28: "grid cell of each city". One grid cell? Given the high resolution of your inner domain, did you release tracers from one grid cell or from a region (city)? Please clarify in the text.

  We release the tracer in a single grid cell for each city. This assumption leads to pollution plumes thinner as the reality. But, given the strong urbanization of the Guinean coastal region, there are anthropogenic emissions almost continuously from Abidjan to Lagos. As we want to distinguish the contribution of the major agglomeration, we release the tracers from a single grid cell.
  The sentence *'The tracer emissions occur in the grid cell of each city.'* has been changed as: *'Specific tracers are emitted for a given city in order to distinguish their relative contributions at inland locations. Thus the tracer emissions occur in a single grid cell of each city corresponding to the center.'*.

- P7-L1: How much tracer did you release? Please clarify how you "reproduce the BB layer observed with MODIS" considering that the tracers are gaseous.

  The quantity of tracer is not important because we use an arbitrary unit. The expression *'reproduce the BB layer observed with MODIS'* meant that we reproduce the spatial extent of the aerosol pattern seen with MODIS AOD and supposed to be associated with a BB layer (Section 3.1).
  The sentence *'In order to analyze the interactions between URB emissions and the BB layer, we reproduce the BB layer releasing passive gaseous tracers from 5 July at 00:00 UTC to 6 July at 23:00 UTC with a spatial horizontal extent from 1^oW to 2^oE at 4.5^oN, and the altitude as suggested by satellite observations (Figure A1) at $\approx$ 1.5 km amsl.'* has been reworded: *'In order to analyze the interactions between URB emissions and the BB layer, we use the information on the spatial characteristics and vertical extent of the BB layer derived from MODIS and CALIPSO observations (Section 3.1) by releasing passive gaseous tracers with a spatial horizontal extent from 1^oW to 2^oE at 4.5^oN and with an altitude of $\approx$ 1.5 km amsl from 5 July at 00:00 UTC to 6 July at 23:00 UTC (cf. Table 3).'*.

- P9-L16: "Section 3.2" Do you mean Section 3.2.1?

  The reviewer is right. It has been corrected.

- P9-L18: Please comment on RH in layer (ii) to be consistent.

  It has been commented in the new version: *'(ii) between 1 to 2 km amsl, there is a directional shear layer associated with high RH $>$ 90 % and with low wind speed and changing wind direction;'*.

- P9-L24: "the first kilometer" is this the monsoon layer? Please be consistent.

  In order to be consistent, we have replaced 'the first kilometer' by 'the monsoon layer'.

- P9-L27: "wind speed is wider than at lower altitudes". Remove "than".

  It has been corrected.

- P10-L18: Did you compare measured and modeled RH? This can help to better understand the model performance in capturing PBL height and (maybe) clouds.

  Observed and modeled RH are compared in Section 3.2. We decided that the comparison of observed and modeled RH is not important for Section 3.3 because we want especially to validate the wind speed and direction in order to accurately reproduce the pollutant transport, which is the focus of our study.

- P11-L1: What is "feature G"?

  This was unclear and unnecessary. 'Feature G' refers to a feature described in Knippertz et al. (2017). The parenthesis *'(described as feature G in this study)'* has been removed.

- P11-L22: NO and NO2 have a short lifetime and are not trace gases.

  That is true. We have replaced *'this section investigates the trace gas concentrations'* by *'this section investigates CO and NO_x concentrations'*.

- P29-Figure 5: Do thick marks indicate 00Z?

  The vertical dashed lines (and the corresponding tick marks) indicate periods of 6 hours starting at 00:00 UTC (00Z). It has been specified in the caption of Figure 5: *'The vertical dashed lines indicate periods of 6 hours starting at 00:00 UTC.'*.

- P12-L14-15: Increase in evening NO2/NO can be due to lower PBL (higher NO2 concentration) and reduction in NO by reacting with O3.

  Close to the sources of incomplete combustion, there is always production of NO. We interpret the NO_2/NO ratio together with the NO concentration in order to confirm that there is no local production. The sentence *'We note every day a sharp increase in the evening (NO_2/NO > 15), which suggests transported pollutants.'* has been modified such as: *'We note every day a sharp increase from 18:00 to 00:00 UTC (NO_2/NO > 15) associated with low NO concentrations (NO < 0.2 ppb), which suggests transported pollutants.'*

- P12-L20: On July 5th concentration of both CO and NOx (more) increased in the evening thus resulted in a decrease in CO/NOx ratio and increase in NO2/NO. Maybe a mixture of BB and URB was transported to Save?

  We have highlighted this fact in the manuscript. It shows that there is no increase of CO without NO_x increase, thus if the BB layer reach Savè, it is mixed with urban pollution.
  The sentence *'At Savè, the CO/NO_x ratio is not higher after the arrival of the BB layer on 5 July (cf. Section 3.1).'* has been modified such as *'At Savè, the CO/NO_x ratio is not higher after the arrival of the BB layer on 5 July (cf. Section 3.1). There is an increase of CO together with a NO_x increase, thus when the BB layer reaches Savè, it is mixed with urban pollution or transported above the PBL.'*

- P12-L23: no need to start a new paragraph.

  OK

- P12-28-29: Could the nighttime increase in CO (and NO2 in the next paragraph) concentrations be due to lower PBL height? Please comment in the text.
- P12-L34: Again, lower nighttime PBL height can also justify the increase in CO and NO2 concentrations.
- P13-L4: or shorter lifetime of NO2?

  For these three points, we think that it would be the case if there are anthropogenic emissions at night in the vicinity of the measurements. During the entire campaign, we did not note any increase of NO at night. We consider that the super-site of Savè is well suited to study pollution transport from the coast to the North because of the low anthropogenic emissions. This information is now provided with a new paragraph in Section 2.2: *'Three super-sites have been implemented in the framework of the DACCIWA project in Kumasi (Ghana), Ile-Ife (Nigeria) and Savè (Benin). Unlike the two others, Savè is representative of transport-related air quality issues affecting small cities, characterized by low local emissions, downstream of large coastal cities. It is ideal in that the terrain is very flat with no orographically induced circulation impacting the monsoonal flow. Thus to study NOx and CO from coastal urbanized areas, this rural environment is well suited.'*
  We understand the question of the reviewer as a question about the relative quantification of several dynamical processes on surface concentrations increases. The question is: *'Observing CO and NO2 surface concentrations increases, is it due to long-range transport of urban plumes and/or local collapse of the nocturnal boundary layer?'*. The answer is that we have shown with the numerical tracer experiments (Section 4.2) that the long-range transport is important for the surface concentration increases at Savè in the evening and could explain entirely these increases.
  In the past paragraph of Section 4.2, this sentence was added: *'The observed increases in surface concentration may be explained by several processes: long-range transport of the URB plume and/or a local collapse of the nocturnal boundary layer, quickly concentrating locally emitted pollutants. In our case, the dominant effect is the long-range transport, which is mainly associated with the transport of the Cotonou plume. Moreover, during the entire campaign, we did not note any increase of NO at night (Figure A4 and A5).'*.

- P12-L32: What about NO peak at 12UTC?

It was missing. It has been added in the sentence: *'The two small NO increases (from 0.2 to 0.6 ppb) at 12:00 and 19:00 UTC are consistent with the usual time of local activities such as traffic and charcoal cook stoves.'.*

- P13-L13: please reference the figure after "single figure"

  OK

- P13-L16: "northwestward" you mean "southwestward"?

  It has been corrected.

- P13-L21: What time did you start releasing the tracers?

  The sentence *'The first tracer plume that reaches Savè typically around 19:00 UTC is from Cotonou.'* has been modified *'The tracer emissions started on 1 July at 00:00 UTC and the first tracer plume that reaches Savè is from Cotonou in the evening. We can see that tracers emitted from Cotonou reach Savè every day in evening, typically at around 19:00 UTC.'*

2.4 References

- Yang, Y., Wang, H., Smith, S. J., Ma, P.-L. and Rasch, P. J.: Source attribution of black carbon and its direct radiative forcing in China, Atmos. Chem. Phys., 17(6), 4319-4336, doi:10.5194/acp-17-4319-2017, 2017.
- Kulkarni, S., et al. "Source sector and region contributions to BC and PM 2.5 in Central Asia." Atmospheric Chemistry and Physics 15.4 (2015): 1683-1705.
- Sobhani, N., Kulkarni, S. and Carmichael, G. R.: Source Sector and Region Contributions to Black Carbon and PM2.5 in the Arctic, Atmos. Chem. Phys. Discuss., 2018, 1-43, doi:10.5194/acp-2018-65, 2018.

  These references have been added to the manuscript.

References

DGSCN report: Quatrime Recensement Gnral de la Population et de lHabitation du Togo - RGPH4, Direction Gnrale de la Statistique et de la Comptabilit Nationale, Ministre de la Planification, du Dveloppement et de lAmnagement du Territoire, URL `http://www.stat-togo.org/contenu/pdf/pb/pb-vol-2-rgph4-tg-2010.pdf, [Accessed:21/03/2018]`, 2016.

Adler, B., Kalthoff, N., and Gantner, L.: Nocturnal low-level clouds over southern West Africa analysed using high-resolution simulations, Atmospheric Chemistry and Physics, 17, 899–910, doi:10.5194/acp-17-899-2017, 2017.

Andela, N. and Van Der Werf, G. R.: Recent trends in African fires driven by cropland expansion and El Niño to la Niña transition, Nature Climate Change, 4, 791–795, doi:10.1038/nclimate2313, 2014.

Deetz, K., Vogel, H., Haslett, S., Knippertz, P., Coe, H., and Vogel, B.: Aerosol liquid water content in the moist southern West African monsoon layer and its radiative impact, Atmospheric Chemistry and Physics Discussions, pp. 1–44, doi:10.5194/acp-2018-420, 2018.

Deroubaix, A., Flamant, C., Menut, L., Siour, G., Mailler, S., Turquety, S., Briant, R., Khvorostyanov, D., and Crumeyrolle, S.: Interactions of Atmospheric Gases and Aerosols with the Monsoon Dynamics over the Sudano-Guinean region during AMMA, Atmospheric Chemistry and Physics, 18, 445–465, doi:10.5194/acp-18-445-2018, 2018.

Flamant, C., Deroubaix, A., Chazette, P., Brito, J., Gaetani, M., Knippertz, P., Fink, A. H., de Coetlogon, G., Menut, L., Colomb, A., Denjean, C., Meynadier, R., Rosenberg, P., Dupuy, R., Schwarzenboeck, A., and Totems, J.: Aerosol distribution in the northern Gulf of Guinea: local anthropogenic sources, long-range transport and the role of coastal shallow circulations, Atmospheric Chemistry and Physics, 18, 12 363–12 389, doi:10.5194/acp-18-12363-2018, 2018a.

Flamant, C., Knippertz, P., Fink, A. H., Akpo, A., Brooks, B., Chiu, C. J., Coe, H., Danuor, S., Evans, M., Jegede, O., Kalthoff, N., Konaré, A., Liousse, C., Lohou, F., Mari, C., Schlager, H., Schwarzenboeck, A., Adler, B., Amekudzi, L., Aryee, J., Ayoola, M., Batenburg, A. M., Bessardon, G., Borrmann, S., Brito, J., Bower, K., Burnet, F., Catoire, V., Colomb, A., Denjean, C., Fosu-Amankwah, K., Hill, P. G., Lee, J., Lothon, M., Maranan, M., Marsham, J., Meynadier, R., Ngamini, J.-B., Rosenberg, P., Sauer, D., Smith, V., Stratmann, G., Taylor, J. W., Voigt, C., and Yoboué, V.: The Dynamics-Aerosol-Chemistry-Cloud Interactions in West Africa field campaign: Overview and research highlights, Bulletin of the American Meteorological Society, 99, 83–104, doi:10.1175/BAMS-D-16-0256.1, 2018b.

Giglio, L., Csiszar, I., and Justice, C. O.: Global distribution and seasonality of active fires as observed with the Terra and Aqua Moderate Resolution Imaging Spectroradiometer (MODIS) sensors, Journal of Geophysical Research: Biogeosciences, 111, 1–12, doi:10.1029/2005JG000142, 2006.

INSAE report: Quatrime Recensement Gnral de la Population et de lHabitation du Bnin - RGPH4, Institut National de la Statistique et de l'Analyse Economique, Direction des Etudes Dmographique, Ministre du Dveloppement, de l'Analyse Economique et de la Prospective, URL `http://www.insae-bj.org/recensement-population.html, [Accessed:21/03/2018]`, 2015.

Janicot, S., Thorncroft, C. D., Ali, A., Asencio, N., Berry, G., Bock, O., Bourles, B., Caniaux, G., Chauvin, F., Deme, A., Kergoat, L., Lafore, J.-P., Lavaysse, C., Lebel, T., Marticorena, B., Mounier, F., Nedelec, P., Redelsperger, J.-L., Ravegnani, F., Reeves, C. E., Roca, R., de Rosnay, P., Schlager, H., Sultan, B., Tomasini, M., and Ulanovsky, A.: Large-scale overview of the summer monsoon over West Africa during the AMMA field experiment in 2006, doi:10.5194/angeo-26-2569-2008, 2008.

Kalthoff, N., Lohou, F., Brooks, B., Jegede, G., Adler, B., Babić, K., Dione, C., Ajao, A., Amekudzi, L. K., Aryee, J. N. A., Ayoola, M., Bessardon, G., Danuor, S. K., Handwerker, J., Kohler, M., Lothon, M., Pedruzo-Bagazgoitia, X., Smith, V., Sunmonu, L., Wieser, A., Fink, A. H., and Knippertz, P.: An overview of the diurnal cycle of the atmospheric boundary layer during the West African monsoon season: Results from the 2016 observational campaign, Atmospheric Chemistry and Physics, pp. 2913–2928, doi:10.5194/acp-2017-631, 2018.

Knippertz, P., Coe, H., Chiu, J. C., Evans, M. J., Fink, A. H., Kalthoff, N., Liousse, C., Mari, C., Allan, R. P., Brooks, B., Danour, S., Flamant, C., Jegede, O. O., Lohou, F., and Marsham, J. H.: The DACCIWA project: Dynamics-aerosol-chemistry-cloud interactions in West Africa, Bulletin of the American Meteorological Society, p. 150203142711003, doi:10.1175/BAMS-D-14-00108.1, 2015.

Knippertz, P., Fink, A. H., Deroubaix, A., Morris, E., Tocquer, F., Evans, M. J., Flamant, C., Gaetani, M., Lavaysse, C., Mari, C., Marsham, J. H., Meynadier, R., Affo-Dogo, A., Bahaga, T., Brosse, F., Deetz, K., Guebsi, R., Latifou, I., Maranan, M., Rosenberg, P. D., and Schlueter, A.: A meteorological and chemical overview of the DACCIWA field campaign in West Africa in JuneJuly 2016, Atmospheric Chemistry and Physics, 17, 10 893–10 918, doi:10.5194/acp-17-10893-2017, 2017.

Kulkarni, S., Sobhani, N., Miller-Schulze, J. P., Shafer, M. M., Schauer, J. J., Solomon, P. A., Saide, P. E., Spak, S. N., Cheng, Y. F., Denier van der Gon, H. A. C., Lu, Z., Streets, D. G., Janssens-Maenhout, G., Wiedinmyer, C., Lantz, J., Artamonova, M., Chen, B., Imashev, S., Sverdlik, L., Deminter, J. T., Adhikary, B., D Allura, A., Wei, C., and Carmichael, G. R.: Source sector and region contributions to BC and PM2.5 in Central Asia, Atmospheric Chemistry and Physics, 15, 1683–1705, doi:10.5194/acp-15-1683-2015, 2015.

Menut, L., Flamant, C., Turquety, S., Deroubaix, A., Chazette, P., and Meynadier, R.: Impact of biomass burning on pollutants surface concentrations in megacities of the Gulf of Guinea, Atmospheric Chemistry and Physics, 18, doi:10.5194/acp-18-2687-2018, 2018.

Redelsperger, J. L., Thorncroft, C. D., Diedhiou, A., Lebel, T., Parker, D. J., and Polcher, J.: The African Monsoon Multidisciplinary Analysis: An International Research Project and Field Campaign, Bulletin of the American Meteorological Society, 87, 1739–1746, 2006.

Reed, C., Evans, M. J., Di Carlo, P., Lee, J. D., and Carpenter, L. J.: Interferences in photolytic NO2 measurements: explanation for an apparent missing oxidant?, Atmospheric Chemistry and Physics, 16, 4707–4724, doi:10.5194/acp-16-4707-2016, 2016.

Reeves, C. E., Formenti, P., Afif, C., Ancellet, G., Attié, J. L., Bechara, J., Borbon, A., Cairo, F., Coe, H., Crumeyrolle, S., Fierli, F., Flamant, C., Gomes, L., Hamburger, T., Jambert, C., Law, K. S., Mari, C., Jones, R. L., Matsuki, A., Mead, M. I., Methven, J., Mills, G. P., Minikin, A., Murphy, J. G., Nielsen, J. K., Oram, D. E., Parker, D. J., Richter, A., Schlager, H., Schwarzenboeck, A., and Thouret, V.: Chemical and aerosol characterisation of the troposphere over West Africa during the monsoon period as part of AMMA, Atmospheric Chemistry and Physics, 10, 7575–7601, doi:10.5194/acp-10-7575-2010, 2010.

Sauvage, B., Thouret, V., Cammas, J.-P., Gheusi, F., Athier, G., and Nédélec, P.: Tropospheric ozone over Equatorial Africa: regional aspects from the MOZAIC data, Atmospheric Chemistry and Physics, 5, 311–335, doi:10.5194/acp-5-311-2005, 2005.

Sobhani, N., Kulkarni, S., and Carmichael, G. R.: Source Sector and Region Contributions to Black Carbon and PM2.5 in the Arctic, Atmospheric Chemistry and Physics Discussions, pp. 1–43, doi:10.5194/acp-2018-65, 2018.

United Nations report: World urbanization prospects: the 2011 revision, Population Division, Department of Economic and Social Affairs, United Nations Secretariat, URL http://www.un.org/en/development/desa/population/publications/pdf/urbanization/WUP2011_Report.pdf, [Accessed:11/06/2018], 2011.

Winker, D. M., Vaughan, M. A., Omar, A., Hu, Y., Powell, K. A., Liu, Z., Hunt, W. H., and Young, S. A.: Overview of the CALIPSO Mission and CALIOP Data Processing Algorithms, Journal of Atmospheric and Oceanic Technology, 26, 2310–2323, doi:10.1175/2009JTECHA1281.1, 2009.

Yang, Y., Wang, H., Smith, S. J., Ma, P.-L., and Rasch, P. J.: Source attribution of black carbon and its direct radiative forcing in China, Atmospheric Chemistry and Physics, 17, 4319–4336, doi:10.5194/acp-17-4319-2017, 2017.

Diurnal cycle of coastal anthropogenic pollutant transport over southern West Africa during the DACCIWA campaign

Adrien Deroubaix[1,2], Laurent Menut[1], Cyrille Flamant[2], Joel Brito[9], Cyrielle Denjean[6], Volker Dreiling[7], Andreas Fink[5], Corinne Jambert[4], Norbert Kalthoff[5], Peter Knippertz[5], Russ Ladkin[8], Sylvain Mailler[1], Marlon Maranan[5], Federica Pacifico[4], Bruno Piguet[6], Guillaume Siour[3], and Solène Turquety[1]

[1]LMD/IPSL, École Polytechnique, Université Paris Saclay, ENS, IPSL Research University; Sorbonne Universités, UPMC Univ Paris 06, CNRS, Palaiseau, France
[2]LATMOS/IPSL, Sorbonne Université, Université Paris-Saclay & CNRS, Paris, France
[3]LISA/IPSL, Laboratoire Interuniversitaire des Systèmes Atmosphériques (LISA), UMR CNRS 7583, Université Paris Est Créteil et Université Paris Diderot, Institut Pierre Simon Laplace, Créteil, France
[4]LA, Laboratoire d Aérologie, University of Toulouse, CNRS, UPS, Toulouse, France.
[5]KIT, Institute of Meteorology and Climate Research, Karlsruhe Institute of Technology, Germany
[6]CNRM, Centre National de la Recherche Météorologique, UMR3589, CNRS, Météo-France, Toulouse, France
[7]DLR, Deutsches Zentrum für Luft-und Raumfahrt, Oberpfaffenhofen, Germany
[8]BAS, British Antarctic Survey, Cambridge, UK
[9]LAMP, Laboratoire de Météorologie Physique, Université Clermont Auvergne, Aubière, France

Correspondence to: Adrien.Deroubaix@lmd.polytechnique.fr

Abstract. During the monsoon season, pollutants emitted by large coastal cities and biomass burning plumes originating from Central Africa have complex transport pathways over Southern West Africa (SWA). The Dynamics-Aerosol-Chemistry-Cloud-Interactions in West Africa (DACCIWA) field campaign has provided numerous dynamical and chemical measurements in and around the super site of Savè in Benin (≈ 185 km away from the coast), which allows quantifying the relative contribution of advected pollutants. Through the combination of in-situ ground measurements with aircraft, radio-sounding, satellite and high-resolution chemistry-transport modeling with the CHIMERE model, the source attribution and transport pathways of pollutants inland (here, NO_x and CO) are carefully analyzed for the ~~01 – 07~~ 01–07 July 2016 period. The relative contributions of different sources (*i.e.* emissions from several large coastal cities) on the air quality in Savè are characterized. It is shown that a systematic diurnal cycle exists with high surface concentrations of pollutants from 18:00 to 22:00 UTC. This evening peak is attributed to pollution transport from the coastal city of Cotonou (Benin). Numerical model experiments indicates that the anthropogenic pollutants are accumulated during the day close to the coast, and transported northward as soon as the daytime convection in the atmospheric boundary layer ceases after 16:00 UTC, reaching 8°N at 21:00 UTC. When significant biomass burning pollutants are transported into continental SWA, they are mixed with anthropogenic pollutants along the coast during the day, and this mixture is then transported northward. At night, most of the coastal anthropogenic plumes are transported within the planetary boundary layer (below about 500 m above ground level), whereas the biomass burning pollutants are mostly transported above it, thus generally not impacting ground level air quality.

1 Introduction

The United Nations Department of Economic and Social Affairs, Population Division reported 31 megacities globally (urban agglomerations with more than 10 million inhabitants in 2016) and that their number is projected to rise up to 41 by 2030. In Southern West Africa (SWA), Lagos is considered as a megacity (with more than 13 million inhabitants) and is expected to reach 24 million in 2030. The urban agglomeration ~~extents~~ extends along the coast to Cotonou (Benin) and even to Lomé (Togo). Moreover Accra in Ghana (with a population predicted to increase from 2.3 in 2016 to 3.3 million in 2030), Kumasi in Ghana (with a population predicted to increase from 2.7 in 2016 to 4.2 million in 2030) and Abidjan in Ivory Coast (with a population predicted to increase from 5.0 in 2016 to 7.8 million in 2030) will all contribute to form a more or less continuously urbanized strip at some point during the ~~21th~~ twenty-first century. This growth is associated with enhanced pollutant emissions and low air quality, which leads to chronic health problems (Lelieveld et al., 2015) and contributes to anthropogenically forced climate change.

The vertical structure of air pollution is complex along the Guinea Coast during the period when the West African Monsoon (WAM) is established in the boreal summer. From the surface to the top of the Planetary Boundary Layer (PBL), marine air transported by the northeastward monsoon flow gets enriched with anthropogenic pollution emitted at the coast before moving further inland (Knippertz et al., 2015b). Above the marine PBL, biomass burning aerosol layers, resulting from incomplete combustion of fires in Central Africa (Giglio et al., 2006; Zuidema et al., 2016) can be observed on occasion reaching the Guinea Coast after being transported over thousands of kilometers (Menut et al., 2018). In higher layers, at altitudes from 3 to 5 km, the Saharan Air Layer (SAL) is generally observed to be advected from the north depending on the meridional disturbances of African Easterly Jet (AEJ), carrying desert dust (Flamant et al., 2009; Crumeyrolle et al., 2011; Lafore et al., 2011). This general picture is often perturbed by the presence of organized convective systems, which propagate along the Guinea Coast from Nigeria to Liberia (Maranan et al., 2018). The latter authors also note the presence of land-sea breeze convective systems in the immediate coastal strip.

The EU-funded project Dynamics-Aerosol-Chemistry-Cloud-Interactions in West Africa (DACCIWA) was designed to focus specifically on the Guinea Coastal atmospheric dynamics and the interactions between aerosols, chemistry and clouds (Knippertz et al., 2015a). An intensive measurement campaign took place in Nigeria, Benin, Togo, Ghana and Ivory Coast during June-July 2016, which corresponds to the climatological onset period of the WAM (Janicot et al., 2008). Three research aircraft flew over the Guinea Coastal region with different scientific objectives, notably with flight plans designed to map out city, shipping and flaring emissions or focused on sampling biomass burning aerosols layers (Flamant et al., 2018b). The DACCWIA field campaign took place in so-called post WAM ~~onset~~ post-onset conditions, *i.e.* after deep convection (and related precipitation) had migrated from the coast, inland over the Sahel (Knippertz et al., 2017).

During the WAM, the atmospheric composition over the Gulf of Guinea coastal region is the result of a complex mix of natural and anthropogenic sources, which include urban, biomass burning, biogenic, desert dust and oceanic compounds. Using numerical tracer experiments, Menut et al. (2018) have highlighted that fire emissions in Central Africa impacting the surface aerosol and gaseous species concentrations over the Gulf of Guinea are mostly transported over the southeast

Atlantic above the marine PBL. Using WRF-CHIMERE numerical simulations of the WAM during the African Monsoon Multidisciplinary Analyses (AMMA) campaign ~~(May –~~period from May to July 2006~~)~~, Deroubaix et al. (2018) quantified the relative contributions of anthropogenic and biomass burning sources to carbon monoxide (CO) concentrations over SWA, which in July ~~is~~ 2006 was about 25 % local anthropogenic and 50 % biomass burning from Central Africa. The remaining 25 % are the background corresponding to long-range transport from outside of Africa. In order to better distinguish the contributions from different sources to background concentrations, additional studies are needed focusing on Africa as it has been done for other regions (e.g. Kulkarni et al., 2015; Yang et al., 2017; Sobhani et al., 2018).. However the high biomass burning contribution is partly due to the significant under-estimation anthropogenic emission for the Gulf of Guinea region (Marais et al., 2014; Marais and Wiedinmyer, 2016; Liousse et al., 2017; Keita et al., 2018).

AMMA was focused on the Sahelian region combining a multi-scale approach to better characterize the interactions between atmosphere, land and ocean during the monsoon (Janicot et al., 2008; Redelsperger et al., 2006), whereas the DACCIWA project is dedicated to the interactions between aerosols, clouds and radiation along the highly urbanized coastline of the Gulf of Guinea (Knippertz et al., 2015a). Over SWA, Adler et al. (2017) and Deetz et al. (2018) have documented a regular occurrence of a coastal front, which is located where the strongest horizontal gradients of wind speed and potential temperature occur. It develops during daytime and propagates inland in the evening. After the frontal passage, the wind in the lowermost troposphere brings air masses from the coast northward, especially at night with the Nocturnal Low-Level Jet (NLLJ) (Schuster et al., 2013), and probably also anthropogenic pollutants emitted from coastal urban areas (e.g. Djossou et al., 2018) and biomass burning pollutants imported by monsoon flow ~~(Haslett et al. , in preparation).~~ (e.g. Reeves et al., 2010).

The main objective of this article is to understand the diurnal cycle of anthropogenic pollutant transport from the coast to the continental SWA. We present numerical tracer experiments made with high-resolution CHIMERE simulations set up in order to separate the contribution of each important urban agglomeration, namely Abidjan, Accra, Lomé, Cotonou and Lagos. We take advantage of the DACCIWA measurements made by the three research aircraft, by an enhanced radio-sounding network, and at the super-site of Savè in central Benin (Knippertz et al., 2015a). The super-site of Savè ~~serves as~~ is a representative location ~~of inland air quality~~ to assess the impact of pollution transport from the coast on the air quality of remote inland cities characterized by low local emissions. We focus on the period ~~1–7 July~~ 1–7 July 2016, during which a case of long-range transport of biomass burning aerosol from Central Africa was observed (Flamant et al., 2018b). We aim at answering the following questions:

– *What is the relative contribution of each coastal urban area to the air pollution at Savè? How does it evolve during the day?*

– *How are biomass burning and anthropogenic pollutants mixed along the coast and inland? Is it usually a mixture of the two pollutions that is transported inland in the PBL?*

This study is focused on one specific period and location. However, the conclusions are representative of a longer time period as meteorological conditions at the coast during the so-called monsoon post-onset period were found to be quite stable for several weeks (Knippertz et al., 2017). Spatially, the results are directly representative of the studied region only, the main goal being to estimate the influence of the emissions from four coastal cities on the atmospheric composition in the lower troposphere over inland Benin. Given the broad southwesterly monsoon flow in the region, a similar transport from coastal pollution inland will likely be found along the most of the Guinea Coast. We shall answer these questions using a synergistic combination of observations and numerical modeling experiments, described in Section 2. Section 3 analyzes the temporal evolution of meteorology and air pollution over a portion of SWA including Ivory Coast, Ghana, Togo, Benin and Nigeria. Then, we focus on Urban Anthropogenic (URB) and long-range Biomass Burning (BB) pollutant transport in Section 4. Conclusions are given in Section 5.

2 DACCIWA project: observations and modeling

In the DACCIWA project, there are strong components on both in-situ observations and modeling. Here, we present all studied sites (2.1), observational datasets used (section 2.2), and numerical simulations performed to analyze the pollution transport pathways (section 2.3).

2.1 Studied sites

We focus on six locations, five major urban agglomeration of the Guinean ~~Coastal~~ coastal region, and one small town, Savè, which is 185 km north of Cotonou (Benin). Table 1 shows the coordinates and the population of the urban agglomerations studied. For Abidjan, Accra, Lomé and Lagos, we present estimations for the year 2015 of the department of social and economic affairs of United Nations ~~.~~ (United Nations report, 2011). In this report, the cities of Abidjan, Accra, Lagos and Lomé are associated with large administrative areas ~~. The population of the Lagos urban agglomeration is controversial because the last census was in 2006 (details therein)~~in contrast to Cotonou.

Comparing Lomé and Cotonou, Lomé has a large administrative area while Cotonou is a city with a very high population density over a small area. ~~According to the General Population and Habitat Census of Togo (2014,), the~~ The population of Lomé is about ~~837~~839,000 inhabitants in the city according to General Population and Habitat Census of Togo (DGSCN report, 2016)and about 1,~~570~~830,000 inhabitants in the administrative state (United Nations report, 2011). Cotonou city is estimated by the World Urbanization Prospects ~~(The 2011 Revision)~~ report to have about 1,086,000 inhabitants (United Nations report, 2011).

According to the General Population and Habitat Census of Benin ~~(2013,),~~ (INSAE report, 2015), the population of Cotonou only slightly increased by 2.09 % over the period 2002-2013 because of the limited possibility of expansion. They note that along the shores of Lake Nokoué the population has increased rapidly, thus forming an agglomeration of 2,194,000 inhabitants, calculated as the sum of the Cotonou district and several cities of the Atlantique district (~~Abomey Calavi~~ Abomey-Calavi and So-Ava) and of the Ouémé district (Seme Kpodji, Porto Novo, Avrankou and Akpro-Misserete).

City	Country	Latitude	Longitude	Elevation	Number of inhabitants
Abidjan	Ivory Coast	5.36°N	4.00°W	50 m amsl	**4 923 000**
Accra	Ghana	5.60°N	0.19°W	30 m amsl	**3 013 000**
Lomé	Togo	6.17°N	1.23°E	10 m amsl	**1 830 000**
Cotonou	Benin	6.36°N	2.38°E	10 m amsl	2 194 000
Savè	Benin	8.03°N	2.49°E	130 m amsl	87 000
Lagos	Nigeria	6.49°N	3.36°E	10 m amsl	**13 121 000**

Table 1. *Characteristics of the studied cities with: country, latitude, longitude, elevation above mean sea level (amsl), and number of inhabitants of urban agglomerations. The population in bold is given for the year 2015 according to World Urbanization Prospects (The 2011 Revision)report (United Nations report, 2011). National general population and habitat census is used to estimate the population of Cotonou and Savè (2013 Census)(INSAE report, 2015).*

2.2 Observational datasets

During the DACCIWA field campaign, several observational platforms were deployed to perform in-situ and remote sensing measurements (Knippertz et al., 2017; Flamant et al., 2018b). In this study, we use datasets acquiered acquired by ground based stations, aircraftsaircraft, radiosondes and satellites. Table 2 gives the main information on each dataset. Figure 1 presents the location of the aircraft flight tracks, and of the stations. Our studied domain is located in the Greenwich Mean Time (GMT). Hence local time is the same as UTC. During the aircraft campaign period, sunrise occurred around 06:00 UTC and sunset around 18:00 UTC.

Datasets	Platform	Variables	Frequency
Ground based station	Savè super-site (8.03°N, 2.49°E) operated by KIT-UPS universities	NO_2, NO and CO concentrations	Raw data: 1 hz Presented: hourly averages
Aircraft	ATR-42, Twin Otter, Falcon operated by SAFIRE, BAS and DLR teams	Relative humidity Wind direction and speed	Raw data: 1 hz Presented: 3-min averages
Radiosonde	Launch sites: Abidjan, Accra, Cotonou, Savè	Wind direction and speed Relative humidity	High resolution 1 hz Presented: 100 m averages
Satellite	MODIS on Terra and Aqua	AOD (550 nm) level 3 (1°x1°)	Daily

Table 2. *Datasets used in this study with acquisition platform, variables and sampling frequency.*

– Ground based station

Three super-sites have been implemented in the framework of the DACCIWA project in Kumasi (Ghana), Ile-Ife (Nigeria) and Savè (Benin). Unlike the two others, Savè is representative of transport-related air quality issues affecting small cities,

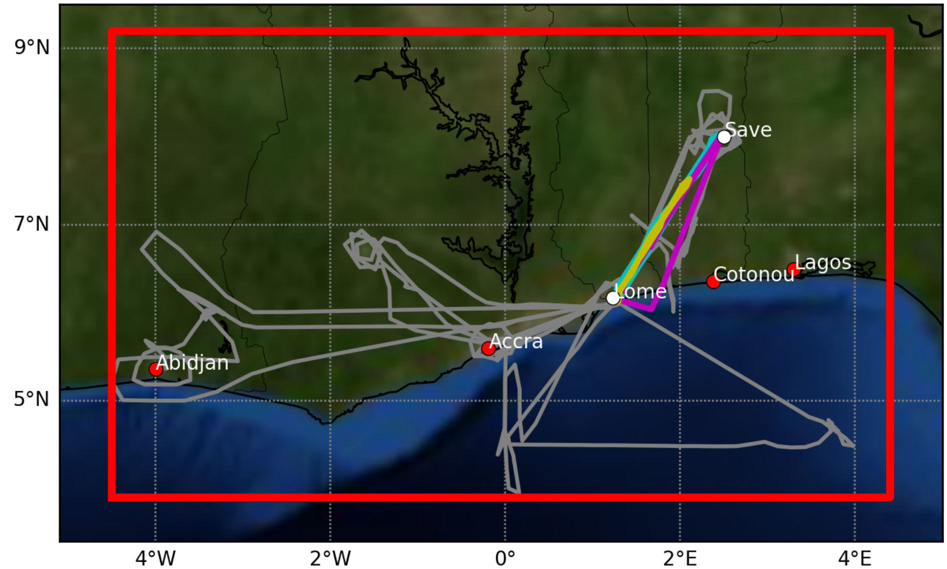

Figure 1. *Map of the modeling domain (red rectangles) with location of the major cities (red dots), of the Lomé airport and the Savè super-site (white dots). Superimposed are the flight tracks of the three research aircraft during the ~~1-7~~ 1–7 July 2016 period (grey lines). The aircraft flight tracks on 5 July are colored for the German Falcon (blue line), the French ATR-42 (violet line) and the British Twin Otter (yellow line).*

characterized by low local emissions, downstream of large coastal cities. It is ideal in that the terrain is very flat with no orographically induced circulation impacting the monsoonal flow. Thus to study NOx and CO from coastal urbanized areas, this rural environment is well suited.

At Savè, the Karlsruhe Institute of Technology (KIT) and the Paul Sabatier University (UPS) have set-up ~~one of the three DACCIWA super-sites~~meteorological and atmospheric composition measurements. UPS installed a chemical analyzer (ThermoEnvironment Instrument) which measured NO_2, NO and CO surface concentrations (Pacifico et al., 2018; Kalthoff et al., 2018). Raw observations acquired at 10 s are averaged hourly. The detection limit of the instrument is 0.05 ppb for NO_2 and NO, and 12 ppb for CO (Derrien and Bezombes, 2016). The measurements site is upwind of the Savè city when the wind corresponds to the monsoon flow (SW sector). On 3 July from 18:00 to 21:00 UTC, the wind direction was shifted, which corresponds to local pollution. This period has been removed from the analysis.

– ~~Aircraft campaign~~

The DACCIWA aircraft campaign took place during the period 25 June - 14 July 2016 and was based at the Lomé (Togo) airport (Flamant et al., 2018b). Three research aircraft were involved: a Twin Otter operated by the British Antarctic Survey (BAS), an ATR-42 operated by the French "Service des Avions Français Instrumentés pour la Recherche en Environment" (SAFIRE), and a Falcon operated by the German "Deutsches Zentrum für Luft und Raummfahrt" (DLR). We base our study on three variables, namely relative humidity, wind direction and wind speed, which are measured by core meteorological instrumentation. The flights trajectories used are depicted in Figure 1. For the three aircraft, raw observations acquired at 1 Hz are averaged over 3-minute time steps.

- ~~Radiosonde campaign~~

The DACCIWA project included a large radiosonde component with locations carefully chosen building on the AMMA radiosonde campaign experiences (Lothon et al., 2008; Parker et al., 2008; Fink et al., 2011; Schuster et al., 2013). We use radiosondes launched from four locations: Abidjan, Accra, Cotonou and Savè (*cf.* Table 1). There were four releases per day at around 00:00 UTC, 06:00 UTC, 12:00 UTC and 18:00 UTC. In Savè, more radiosondes were launched every 1.5 to 3 hours at the super-site during the Intensive Observation Period of ~~1-7~~ 1–7 July 2016 ~~,~~ (Kalthoff et al., 2018).

- ~~MODIS sensor~~

We analyze the horizontal spatial extent of ~~BB layers~~ the main aerosol plumes from satellite observations of Aerosol Optical Depth (AOD) at 550 nm made by MODIS (MODerate-resolution Imaging Spectroradiometer) on both the Aqua platform (MYD08-D3-6 dataset DOI: https://10.5067/MODIS/MYD08_D3.061, passing over the studied region at 13:30 UTC) and the Terra platform (MOD08-D3-6 dataset DOI: https://10.5067/MODIS/MOD08_D3.061, passing over the studied region at 10:30 UTC). Daily MODIS AOD averages at 1° resolution have been calculated from the Collection 6 combined product of the Dark-Target retrieval available over oceans or non-bright continental surface, and the Deep-Blue retrieval available over deserts (Hsu et al., 2013; Sayer et al., 2013, 2014).

- ~~CALIOP sensor~~

In order to identify the altitude of aerosols together with their speciation, we use the space-borne Cloud-Aerosol Lidar with Orthogonal Polarization (CALIOP) ~~with~~ aerosol type classification (Winker et al., 2009). This classification is suited and accurate to distinguish homogenous aerosol plumes with different optical properties such as sea salt, dust and BB (e.g. Menut et al., 2018). The CALIOP cross-sections are very useful since this is a realistic way to have an instantaneous evaluation of the aerosol layer altitudes, with their type depending on backscattered optical measurements, ~~*e.g.*~~ (e.g. Winker et al., 2013). Data are available on https://www-calipso.larc.nasa.gov/products/lidar/browse_images.

2.3 Numerical modeling by WRF-CHIMERE models

The WRF-CHIMERE simulations presented in this study have a similar set-up to those used by Deroubaix et al. (2018). Both models are run offline in a nested configuration on the same grids ~~. Two nested domains are used over the period 1 to 7 July~~with two domains: a regional domain (10 km×10 km, extending from 1°S to 14°N and from 11°W to 11°E) and a high-resolution coastal domain (2 km×2 km). The simulations over the regional domain are started on 1 June 2006. In the following, we present only results modeled over the high-resolution domain ~~. The studied period~~ (Figure 1). The simulated period over the high-resolution domain (1 to 7 July) is entirely included in ~~a~~ the 2016 WAM post-onset phase, which has been defined from 22 June to 20 July 2016 by Knippertz et al. (2017).

2.3.1 Meteorological fields from the WRF model

Meteorological variables are modeled with the regional non-hydrostatic WRF model (version 3.7.1, Skamarock and Klemp, 2008). The domains have a constant horizontal resolution with 32 vertical levels from the surface to 50 hPa, including about 10 vertical levels below 1 km amsl. We use a 2-way nesting for the communication between different domains.

Global meteorological fields are taken from the US Global Forecast System (operational final analyses) produced by the National Center for Environmental Prediction (ds083.3 dataset DOI: https://10.5065/D65Q4T4Z). These fields are used to provide meteorological initial and boundary conditions, and to nudge hourly fields of pressure, temperature, humidity and wind in the WRF simulations, with spectral nudging, which has been evaluated for regional models by von Storch et al. (2000). In order to enable the PBL variability to be resolved by WRF, low frequency spectral nudging is used only above 850 hPa.

The WRF model set-up is as follows: The microphysics scheme is the Single Moment-6 class microphysics scheme (WSM6), the radiation scheme is the Rapid Radiative Transfer Model for General Circulation Models (RRTMG) with the Monte-Carlo Independent Column Approximation (McICA) method of random cloud overlap from Mlawer et al. (1997), the PBL physics are computed using the Yonsei University scheme (Hong et al., 2006), the cumulus parametrization is the ensemble Grell-Dévényi scheme , (for the high-resolution domain, convective precipitation is explicitly calculated and not parametrized), the surface layer scheme is the Carlson-Boland viscous sub-layer and the surface physics is calculated with the 'Noah' Land Surface Model scheme with four soil temperatures and moisture layers (Ek et al., 2003). This set-up has already been used by Deroubaix et al. (2018) because it allows to reproduce a satisfactory diurnal cycle of wind speed over SWA according to Schuster et al. (2013).

2.3.2 Gaseous tracers transport from the CHIMERE model

CHIMERE is a regional chemistry-transport model (version 2017), fully described in Menut et al. (2013) and Mailler et al. (2016). The 32 vertical levels of the WRF model are projected onto the 20 levels for CHIMERE from the surface and up to 200 hPa.

In this study, the model is used in its tracer version and there is no atmospheric chemistry. We choose to release passive gaseous tracers in the simulation, because we want to analyze only their transport (no chemistry, no deposition) caused by the monsoonal flow. Since we want to distinguish the relative contribution of the pollution of several cities several coastal cities to the pollution further inland, we designed a first experiment for which we impose pseudo-anthropogenic the tracer emissions at specific urbanized locations: Abidjan (Ivory Coast), Accra (Ghana), Lomé (Togo), Cotonou (Benin), Lagos (Nigeria) (*cf.* Table 1 for coordinates). Specific tracers are emitted for a given city in order to distinguish their relative contributions . at inland locations. Thus the tracer emissions occur in a single grid cell corresponding to the center of each city.

The city tracer emissions are constant and continuous during the modeled period (1–7 1–7 July). This allows quantifying the variability due to the meteorology only. The tracer emissions occur in the grid cell of each city. Emissions are released at the lowest level of the model (below 10 m altitude) . Emissions and are proportional to the population of each city, that approach has also been used by Flamant et al. (2018a). We defined an arbitrary emission for one million inhabitants. Then we multiply this emission by a factor depending on the population (*cf.* Table 1): 1.8 for Lomé, 2.2 for Cotonou, 3 for Accra, 5 for Abidjan and 13 for Lagos.

A second objective is to understand the interactions between ~~URB and BB~~ urban (URB) and biomass burning (BB) pollutants resulting from long-rang transport on 5 July. For this, we design a second numerical tracer experiment in which BB tracers are added to the URB tracers, and are tagged to be different from the URB tracers. BB tracers are released to reproduce the BB layer observed with MODIS on 5 July at 00:00 UTC to 6 July at 23:00 UTC with a spatial horizontal extent going from 1°W to 2°E at 4.5°N, and at an altitude of ≈ 1.5 km (*cf.* Figure 9, and Sections 3.1 and 4.3 for justifications).

The two tracer experiments are summarized in Table 3. They are accessible on the DACCIWA database (http://baobab.sedoo.fr/Data-Search/?datsId=1760&project_name=DACCIWA).

	Tracer Experiment 1	**Tracer Experiment 2**
Tracer type	URB tracers only	BB and URB tracers
Release duration	~~1-7~~ 1–7 July	~~5-7~~ 5–7 July (BB) and ~~1-7~~ 1–7 July (URB)
Release altitude	lowest level	at 1500 m (BB) and lowest level (URB)
Release location	5 cities	from 1°W to 2°E at 4.5°N (BB) and 5 cities (URB)
Number of tracer	5 (each city)	2 (BB and URB)

Table 3. *Main characteristics of the two numerical tracer experiments using high resolution modeling at 2-km grid spacing with tracer emissions relevant for biomass burning (BB) and urban pollutants (URB).*

The tracers are transported using the van Leer scheme (van Leer, 1979). There is no sink for tracers (no deposition and no chemical reaction). The tracers are chosen to be gaseous and are representative of the gaseous part of the URB emissions and the BB plume. This choice of gaseous tracers was made to be consistent with the gaseous concentrations measured by the aircraft and the surface gaseous concentrations measured at the Savè super-site. The period is not associated with widespread rain. At Savè, there were only some small precipitation events (Kalthoff et al., 2018). We focus our analysis on gaseous species but we suppose similar transport patterns for aerosol and gaseous pollutants because of the constant monsoon flow blowing over SWA during our studied period. The only difference to aerosol is the absence of settling. But this long-term impact could be considered as negligible in this study focused on a few days and a spatially restricted region: it is assumed that gaseous and aerosol species are transported in the same way by the meteorological flow.

3 Large scale atmospheric patterns over the Gulf of Guinea

This section is dedicated to analysis of the atmospheric dynamics, thermodynamics and composition across SWA using AOD from satellites in Section 3.1, together with relative humidity and wind from radiosondes in Section 3.2 and from aircraft in Section 3.3. The prerequisite to realistic numerical tracer experiments is the accuracy of the meteorological simulation.

The WRF meteorological simulation is therefore extensively compared to in-situ observations made by both radiosondes and aircrafts.

3.1 Regional scale aerosol distribution

This section investigates the daily ~~MODIS-AOD~~ MODIS AOD observations for the period 1 to 7 July 2016. Two important types of aerosols can be advected towards SWA: Dust from the north and BB from the south. We focus on two different days, 3 and 5 July 2016 (Figures 2 and AA1). Note that we present one day moving averages (Figures 2) because we analyze the long-range transport of aerosols (using MODIS level-3 product with a coarse resolution of 1°).

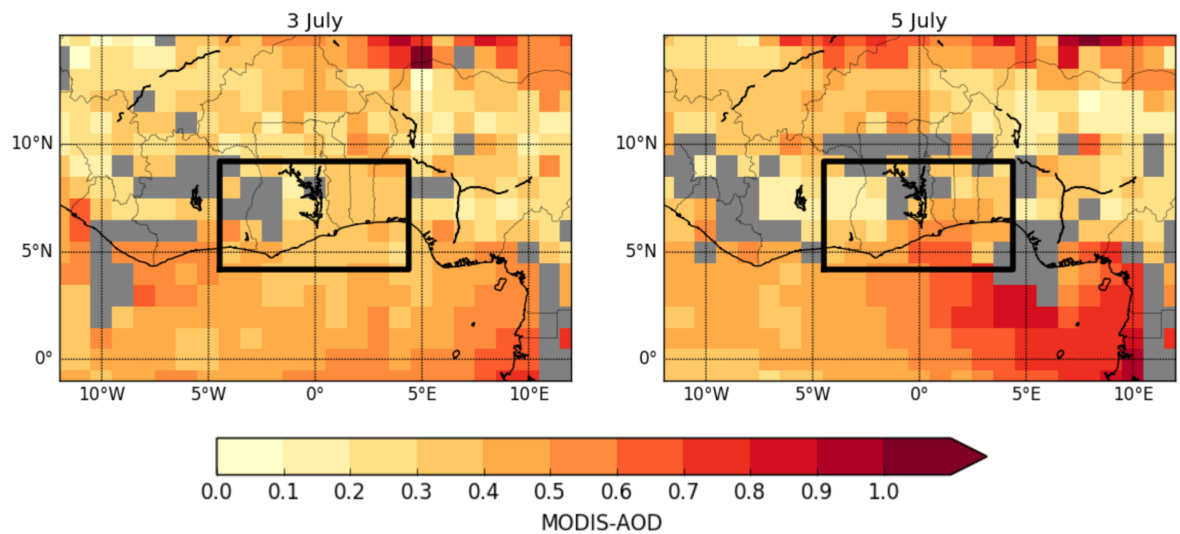

Figure 2. *~~MODIS-AOD~~ MODIS AOD 1-day moving average of two products acquired by Aqua and Terra (the combined Dark-Target and Deep-Blue MYD08-D3 and MOD08-D3 products respectively) on 3 July 2016 (left) and 5 July 2016 (right). Data excluded by the cloud screening process are in gray. The modeling domain is presented by the black square.*

During the studied period, high AOD values are found north of the domain over the Sahel (north of 14°N) and south of the domain over the Gulf of Guinea (on average over the period ~~1–7~~ 1–7 July, Figure AA1). The origin of the high AOD over the Gulf of Guinea is well known. This is the BB layer coming from Central Africa, where intense vegetation fires occur during this season (Giglio et al., 2006) with increasing trends over the period 2001-2012 (Andela and Van Der Werf, 2014). Part of this pollution is transported over the Gulf of Guinea and the BB plume reaches the Guinea Coast ~~depending~~ was seen during the AMMA campaign (Sauvage et al., 2005; Reeves et al., 2010). The BB pollutant concentrations observed along the Guinea Coast depend on the synoptic wind patterns (Menut et al., 2018). The presence of this layer is confirmed over the Gulf of Guinea using CALIPSO data acquired on 5 July (Figure AA2), which gives a layer altitude between 1 and 3 km above mean sea level (amsl). It is worth noting that during this period, there is no evidence of mineral dust transport over the studied cities.

3 and 5 July 2016 are two contrasting days in terms of AOD values over the Gulf of Guinea (Figure 2). On 2 July, AOD values are low over the continent and moderate over the ocean (Figure AA1), which is in agreement with Flamant et al. (2018a) who have shown that the BB layer is present close to the ~~Guinean coast~~ Guinea Coast but it is not reaching the coast. On 3 July, AOD values are low to moderate over our domain (AOD < 0.5, Figure 2). On 4 July, there is a pattern of high AOD (AOD $>$ 0.5) 100 km south of the coast (Figure AA1). On 5 July, the BB layer reaches the coastline (Figure 2), then on 6 July it seems to penetrate inland but clouds prevent AOD retrievals over Togo and Benin (Figure AA1). On 7 July, this layer is no longer visible close to the Guinea Coast (Figure AA1).

For 6 July, Flamant et al. (2018b) have shown a clear large-scale BB signature between Abidjan and Accra with in-situ measurements made onboard the research aircraft. Moreover Brito et al. (2018) have analyzed atmospheric chemistry and demonstrated mixing of urban pollutants with advected BB into the region. This interpretation has been supported by backward trajectories locating the origin of the BB plume in Central Africa. ~~The presence of this layer is also confirmed over the Gulf of Guinea using CALIPSO data acquired on 5 July (Figure A2), which gives a layer altitude between 1 and 3 km above mean sea level (amsl).~~

3.2 Vertical ~~layer identification~~layers in the lowermost troposphere

In this section, we combine observations from the high-resolution radiosondes (Section 3.2.1) and the three aircraft (Section 3.2.2) over the period ~~1–7~~ 1–7 July. For radiosondes, we analyze 32 vertical profiles in Abidjan, 32 in Accra, 26 in Cotonou and 51 in Savè (Figure 3). For aircraft data, we analyzed eleven flights including six of the ATR-42, four of the Falcon and one of the Twin Otter (Table 4). Aircraft observations are acquired only during daytime. The modeled and observed dynamical and thermodynamical variables are compared in order to identify the different layers. The modeled variables have been interpolated along the balloon trajectories and aircraft flight tracks using a spatial bilinear interpolation, and then temporal and vertical linear interpolations with a 3-minute time step.

3.2.1 ~~From~~ Identification from radiosondes

For wind speed, the vertical profiles observed at the four locations have a similar shape (Figure 3). The mean wind speed increases from the surface to 300 m amsl, then decreases to 3 m.s^{-1} at 1.5 km amsl and finally increases to a maximum of about 8 m.s^{-1} between 3 and 5 km amsl. The model predicts a vertical wind profile in good agreement with observations from the surface to 300 m amsl but there is an increasing positive bias from 300 m to 1 km amsl, reaching +2 m.s^{-1} at 1 km amsl. At 300 m amsl, observed wind speed reaches 6 m.s^{-1} on average, which shows the NLLJ signature (Schuster et al., 2013). The model reproduces this signature with wind speed reaching 7 m.s^{-1} but over-estimates its altitude (at 400 m amsl) at the three coastal sites (Abidjan, Accra, Cotonou).

The vertical profile observed at Savè stands out from the three other cities with lower wind speed below 1 km and higher wind speed above 2 km amsl. The lower wind speed near the surface may be related to the greater distance from the coast resulting in a stronger deceleration by friction, which is not reproduced by the model. When looking at 3 km amsl, this is close to the altitudinal maximum of the AEJ. Savè is located at a latitude closer to the AEJ core, which is seen at about 10°N

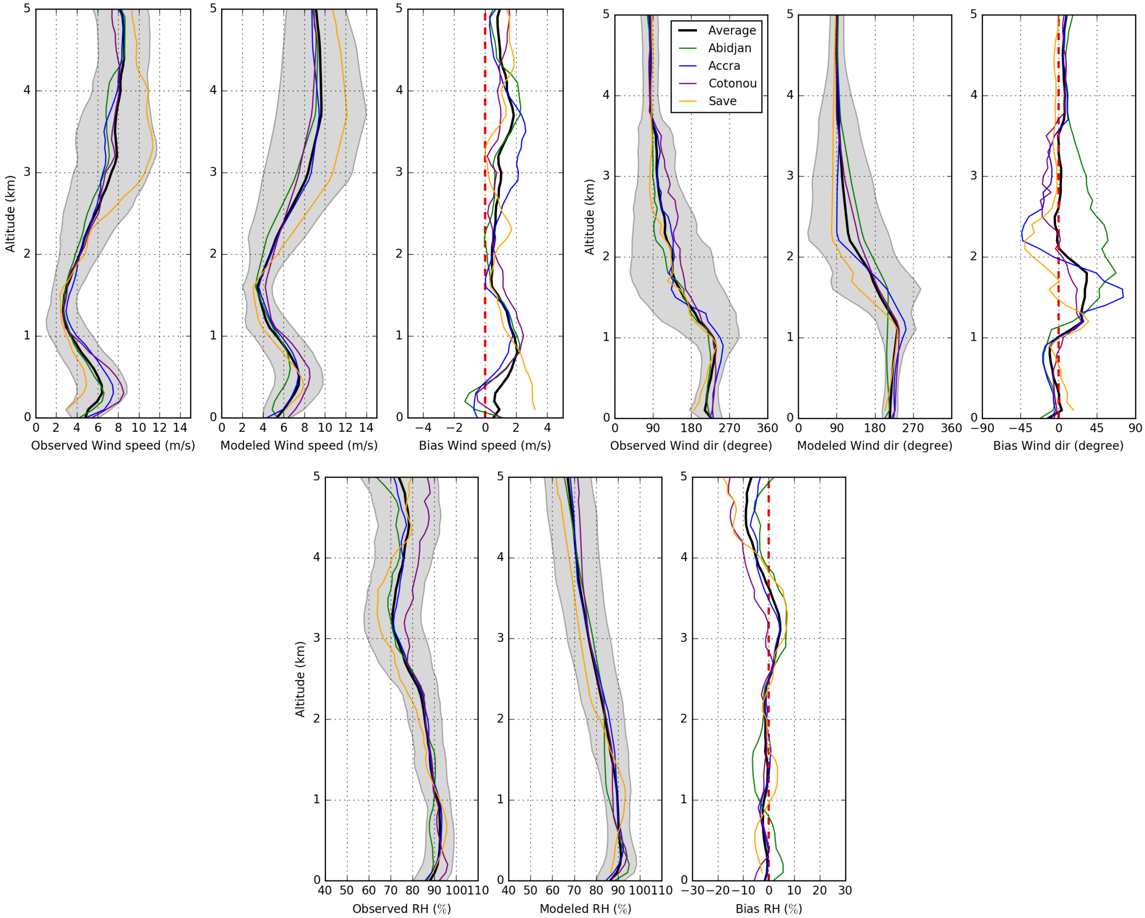

Figure 3. *Observed and modeled mean vertical profiles of wind speed (in m.s^{-1}) and direction (360° circle with 0° and 360° is the north and 90° is the east), and relative humidity (RH in %) averaged of all profiles over the period ~~1-7~~ 1–7 July 2016 at Abidjan in Ivory Coast (green line), Accra in Ghana (blue line), Cotonou in Benin (purple line) and Savè in Benin (orange line). The mean and standard deviation at the four locations are represented by the black line and the gray shading. WRF-derived variables are interpolated to the radiosonde positions. The right panel presents the (mod-obs) mean vertical bias of each location and of the average of the four locations.*

(Knippertz et al., 2017). The jet is clearly observed only at Savè, with wind speeds up to 10 m.s^{-1} at 3 km amsl, which is modeled in good agreement.

For wind direction, the four cities have again similar profiles. The mean observed and modeled vertical profiles are composed of three distinct layers. From the surface to 1 km amsl, the monsoon layer corresponds to wind coming from the sector between 210° and 240°. From 2 to 5 km amsl, wind direction is also almost constant between 80° and 120°. In between these two layers, which are well defined in terms of direction, there is a layer characterized by a quick change of direction from 240° to 120°.

This layer associated with weak wind speed is a directional shear layer. On average, the monsoon layer depth seems to be over-estimated by about 200 m because the modeled wind direction is biased by about +20° between 1.2 and 2 km amsl.

For the three variables, the profiles of their standard deviation present the same modeled and observe characteristics (gray shading in Figure 3). For wind speed, the standard deviation is about 2 $m.s^{-1}$ from the surface to 2 km amsl, and it increases up to 4 $m.s^{-1}$ from 2 to 4 km amsl. For wind direction, the standard deviation is low (about 45°) from the surface to 1 km amsl, it increases from 1 to 2 km in the directional shear layer and it decreases from 2 to 4 km amsl. For RH, the standard deviation is about 10 % from the surface to 2 km amsl, and it increases in the AEJ layer but the model does not reproduce the low RH observed values in this layer.

This analysis shows that the modeled monsoon layer is too deep when it arrives at the coast. Further inland the monsoon flow is too fast when it reaches Savè. The comparison between observed and modeled meteorology also reveals that the model reproduces well enough the several vertical layers in terms of wind direction and speed, and thus most likely the transport that we want to characterize using the tracer experiments.

3.2.2 ~~From~~ Identification from research aircraft

The atmospheric vertical structure can be separated into three different layers (*cf.* Section ~~3.2~~3.2.1): (i) from the surface to 1 km amsl, there is the monsoon flow with RH > 90 %, wind speed > 4 $m.s^{-1}$ and direction from the southwesterly sector; (ii) between 1 to 2 km amsl, there is a directional shear layer associated with high RH > 90 % and with low wind speed and changing wind direction; (iii) between 2 and 4 km amsl, this is the AEJ layer with RH < 80 %, reversed wind direction coming from the northeast and wind speed up to 8 $m.s^{-1}$. In order to evaluate the model, aircraft measurements during daytime are separated into three corresponding altitude ranges (Table 4).

From the surface to 1 km amsl, the modeled wind speed and direction match well with the observations (absolute bias lower than 0.2 $m.s^{-1}$ and 4°, respectively). The observed distribution of the monsoon wind is captured by the model up to 1 km amsl (inter-quartile range 3.80 – 6.47 $m.s^{-1}$ for the observations and 3.98 – 6.80 $m.s^{-1}$ in the simulation). The modeled distribution of RH shows a dry bias in the monsoonal flow (of -6 %).

In the directional shear layer, from 1 to 2 km amsl, ~~modeled wind~~ observed and modeled wind speed distributions are narrower than in the monsoon layer (inter-quartile ranges being 2.10 – 4.04 $m.s^{-1}$ and 1.88 – 3.94 $m.s^{-1}$ respectively), showing that this layer is well defined over the domain. The modeled wind direction is in good agreement with observations (relative bias lower than 1 %), although with a wider distribution (observed inter-quartile range 191.17 ~~—~~– 285.29° and modeled 214.17 ~~—~~– 237.67°) than in the ~~first kilometer~~ monsoon layer (observed inter-quartile range 220.08 ~~—~~– 244.41° and modeled 207.29 ~~—~~– 272.28°). ~~The modeled and observed wind speed distributions are narrower than in the monsoon layer (observed inter-quartile range 2.10 — 4.04 $m.s^{-1}$ and modeled 1.88 — 3.94 $m.s^{-1}$), showing that this layer is well defined over the domain.~~

In the main easterly layer, from 2 to 4 km amsl, the observed distribution of wind speed is wider ~~than~~ at lower altitudes, which is in good agreement with the modeled distribution. Observed and modeled RH and wind direction distributions are also consistent.

Var	N	Q1		Median (Q2)		Q3		Mean		Bias	
		Obs	**Mod**	**Obs**	**Mod**	**Obs**	**Mod**	**Obs**	**Mod**	**Absolute**	**Relative (%)**
0 to 1 km											
RH	349	90.75	85.24	94.80	88.65	98.61	93.50	94.19	88.12	-6.07	-6 %
W. speed	349	3.80	3.98	5.25	5.55	6.47	6.80	5.31	5.51	0.19	4 %
W. dir.	349	220.08	214.17	229.43	228.47	244.41	237.67	231.78	228.19	-3.59	-2 %
1 to 2 km											
RH	116	91.41	88.10	95.58	90.85	98.77	94.79	94.33	90.86	-3.47	-4 %
W. speed	116	2.10	1.88	2.90	2.80	4.04	3.94	3.30	3.04	-0.26	-8 %
W. dir.	116	191.17	207.29	244.71	246.59	285.29	272.28	228.56	228.41	-0.15	>1 %
2 to 4 km											
RH	62	76.34	73.99	84.43	76.86	90.44	85.18	76.12	79.63	3.51	5 %
W. speed	62	3.34	2.23	4.71	5.69	9.08	9.75	6.37	6.67	0.30	5 %
W. dir.	62	55.73	45.76	72.12	69.04	137.67	145.84	107.36	105.24	-2.12	-2 %

Table 4. *Observed and modeled distribution (first quartile, median, third quartile), mean and bias (absolute and relative) of relative humidity (%), wind direction (deg) and speed (m.s^{-1}) measured by the three aircraft over the period ~~1–7~~ 1–7 July 2016 separated into three altitude ranges: surface to 1 km, 1 to 2 km and 2 to 4 km amsl, respectively.*

~~From the surface to 1 km amsl, the modeled wind speed and direction match well the observations (absolute bias lower than 0.2 m.s^{-1} and 4°, respectively). The observed distribution of the monsoon wind is captured by the model up to 1 km amsl (observed inter-quartile range 3.80 — 6.47 m.s^{-1} and modeled 3.98 — 6.80 m.s^{-1}). The modeled distribution of RH shows a dry bias of the model in the monsoon flow (absolute bias of -6 %).~~

~~During~~ In conclusion, during daytime, the monsoon layer is reproduced with a dry bias. The low (relative) biases of wind speed (+4 %) and direction (-2 %) in this layer are of prime importance to accurately model the URB transport.

3.3 From the coast to the North: 5 July Lomé-Savè flights

As we want to understand northward pollution transport, we need to focus on the wind direction and speed from the coast to the north. In this section, we analyze the spatial variability of the wind over the Lomé–Savè transect. We compare aircraft measurements of wind to modeled values using data acquired during three specific flights conducted on 5 July at different times of day with similar flight plans (*cf.* Figure 1) and similar altitude ranges (*i.e.* flying mostly below 2 km amsl). The French ATR-42 flight took place between 08:00 and 11:00 UTC, that of the German Falcon between 11:20 and 15:00 UTC, and that of the British Twin Otter between 16:00 and 17:50 UTC.

Using ceilometer measurements, Flamant et al. (2018b) have described the cloud base height evolution on 5 July at Savè, which was between 200 and 1000 m during the ATR-42 fight, between 400 and 1800 m during the Falcon flight, and between

1000 and 3800 m during the Twin Otter flight. This was a cloudy day, which allowed the operational center to plan for characterizing the diurnal cycle of low level clouds (Flamant et al., 2018b).

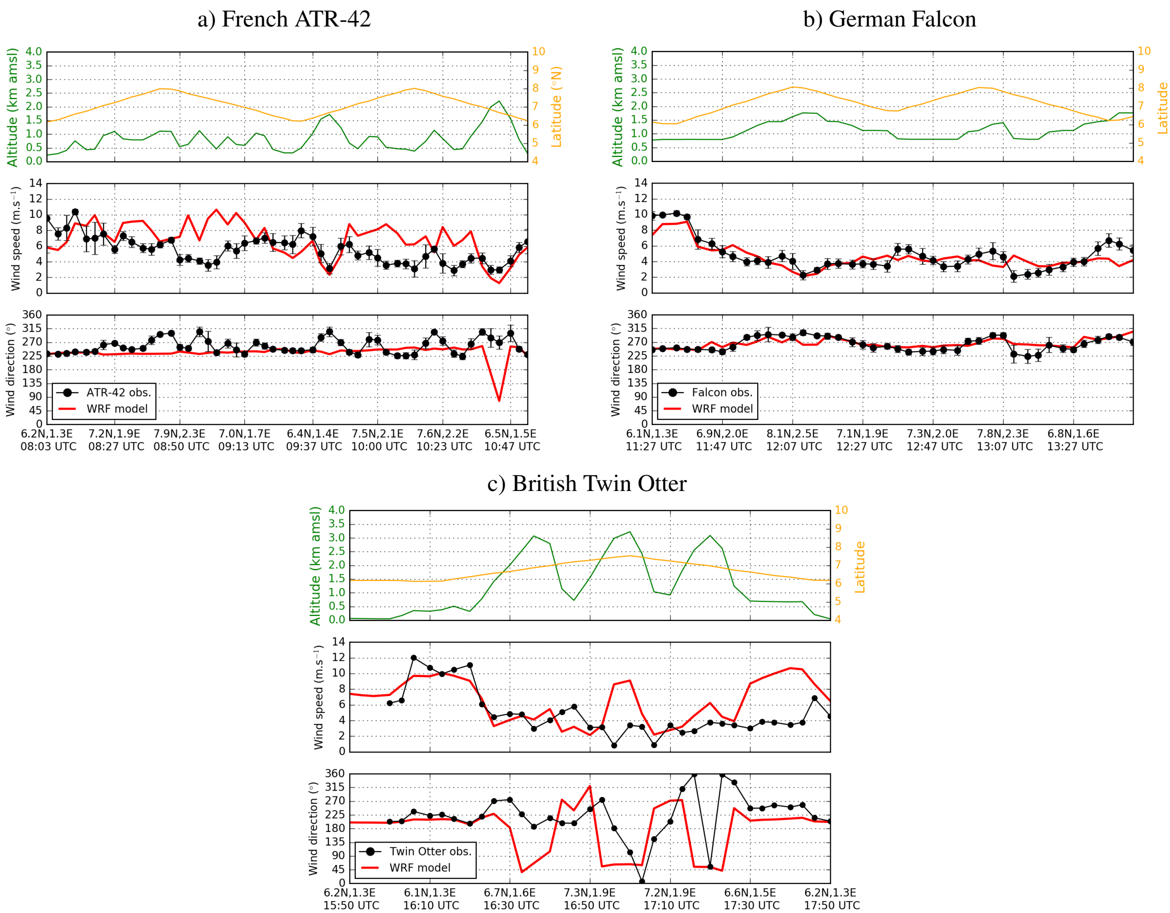

Figure 4. *Time series on 5 July 2016 of (a) the French ATR-42, (b) German Falcon and (c) British Twin Otter aircraft data, composed of three panels for each aircraft: (top) altitude (in m) with the latitude (in °N), (middle) wind speed (in m.s^{-1}) and (bottom) direction (in degree). Modeled values with the WRF model are interpolated along the flight positions (red line). Observed value averages are the black dots with the hourly standard deviation (error bars).*

During the ATR-42 flight in the morning, measurements of wind speed range from 2 to 10 m.s^{-1} (Figure 4). The highest values are observed close to the coast (greater than 8 m.s^{-1}) during the two times the aircraft passes there. The model reproduces the spread of the observed values below 2 km amsl. When the altitude reaches 2 km amsl, observed wind speed decreases below 4 m.s^{-1}. Wind direction ranges from 240° to 300°, even at about 2 km amsl. The model predicts a constant direction at 250°, except when flying above 2 km amsl because the modeled direction changes, revealing an under-estimation of the modeled PBL depth.

In the morning, the monsoon layer is modeled with an over-estimation of the wind speed and with a sharp directional shear at 2 km amsl, whereas we observe an important variability of wind speed without reaching the directional shear layer up to 2 km amsl. This behavior of the model suggests that low level clouds are not well represented, leading to modeled PBL depth under-estimation.

During the Falcon flight around midday, wind speed also decreases from the beginning of the flight at the coast (up to 10 $m.s^{-1}$) to 100 km further North (less than 4 $m.s^{-1}$). Wind direction varies smoothly from 250° at the coast to 300° close to Savè. The model is able to reproduce the weakening of the monsoon layer linked to daytime dry convection (Adler et al., 2017; Deetz et al., 2018), and the variability of observed and modeled wind direction and speed are in better agreement.

In contrast to the ATR-42 and Falcon flights, the Twin Otter flew only one time over Savè and made three vertical profiles up to 3 km amsl. During the Twin Otter flight in the afternoon, the range of wind speed increases compared to the two previous flights, reaching between 1 and 12 $m.s^{-1}$. The model reproduces well the wind in the monsoon layer but does not capture the wind direction changes between 1 and 3 km amsl. There is no clear change of the direction during the first sounding, but during the latter two soundings, wind direction changes from southwesterly winds at 1 km amsl (about 225°) to northeasterly winds at 3 km amsl (about 45°). The model predicts a too sharp wind direction change from 1 to 3 km amsl, which shows that the directional shear layer depth is under-estimated.

Overall below 1 km amsl, wind speed ranges from 4 to 10 $m.s^{-1}$ with a direction from about 250°, which is in good agreement with the model. Knippertz et al. (2017) have shown that 5 July was during a period when the AEJ weakens and becomes more fragmented, which has led to relatively patchy signals in wind and vorticity(described as feature G in this study). This results in observed wind direction mostly greater than the third quartile of the distribution measured over the period 1–7 1–7 July 2016 (Q3=244° below 1 km amsl, *cf.* Table 4).

The three aircraft cover the same region from 08:00 to 17:00 UTC. It is thus possible to quantify the evolution of dynamical variables during daytime. We have selected a box crossed many times by the aircraft in order to compare hourly averages of in-situ wind speed and direction observations to the modeled values. The box is delimited in latitude from 6.6 to 7.8°N, in longitude from 1.5 to 2.2°E and in altitude from 300 to 1000 m amsl (Figure AA3). When the three flights cross this box, the average and standard deviation are calculated from observed values. For the model, we present the average and standard deviation of each hour calculated from all grid cells included in the box.

Wind speed observations decrease from 08:00 to 13:00 UTC (Figure AA3), then increase again in the afternoon (but there are only few measurements made by the Twin Otter aircraft in the two boxes at 17:00 UTC). The model does not capture well the morning evolution, when the NLLJ is eroded. We note that the minimum of wind speed is modeled and observed in the early afternoon, when vertical mixing is strongest. Observed wind directions are almost constant in the box at about 225°. There is a change of the direction between 16:00 and 18:00 UTC for both the model and the observations, which shows the establishment of the NLLJ.

On the one hand, these comparisons with aircraft measurements reinforce our confidence in the model to reproduce adequately the wind speed and direction, thus the main characteristics of pollution transport between Lomé and Savè. On the other hand, this analysis confirms that the PBL depth is not accurately modeled especially in the morning, which could in turn impact the pollution mixing and dilution. During the day, the surface concentration could be over-estimated and the concentration at the PBL top height under-estimated, especially going further away from the sources.

4 Inland pollution transport from coast

Firstly, this section investigates ~~the trace gas~~ CO and NO_x concentrations at the Savè super-site (Section 4.1). Secondly, we analyze the contribution of the major cities along the coastline to the pollution budget in Savè (Section 4.2). Thirdly, we study how URB plumes and the BB layer observed on 5 July interact at the coast and are transported inland.

4.1 Surface pollutant concentrations at Savè

We analyze the temporal evolution of CO, NO_2 and NO concentrations. Trace gas concentrations were measured at the ground level at the Savè DACCIWA super-site. We study the hourly temporal variability of observed concentrations over the studied period (1 to 7 July).

During this period, the hourly CO concentration varies between 140 to 250 ppb (Figure 5-top). Moreover, looking at the entire campaign period (25 June to 15 July), hourly CO concentration ranges from 110 to 250 ppb (Figure AA4-top). Comparing these two periods, we note that our studied period seems representative for the diurnal cycle over the campaign period. There is a clear diurnal cycle with the maximum occurring every day at the beginning of the night (between 220 and 250 ppb) and the minimum at the beginning of the day.

Hourly NO_2 concentration ranges from 0.2 to 3.5 ppb. We note also that every day there are periods of high NO_2 concentrations in the evening and low NO_2 concentrations from the morning to the afternoon. It is worth noting that high CO values noticed in the evening are associated with high NO_2 but not with high NO concentrations.

Given the short lifetime of NO (less than one hour) in the PBL (Monks et al., 2009), the analysis of NO concentration gives some clues to understand NO_2 variability because NO is mostly linked to local sources (*i.e.* not transported). The baseline of NO concentration is 0.09 ppb (median). High NO concentrations ($>$ 0.5 ppb) are measured on 1 and 7 July in the evening. Moreover, there is an increase every evening, which shows that there are local sources close to the instrument location, probably associated with charcoal stove cooking or traffic time.

In order to identify periods of high NO_2 associated with low NO concentrations, we have computed the NO_2/NO ratio (Figure 5-bottom). This ratio is expected to increase at night by the ozone titration (O_3 + NO reaction). During daytime, it depicts local or transported pollution (respectively a low or high NO_2/NO ratio). We note every day a sharp increase ~~in the evening~~ from 18:00 to 00:00 UTC (NO_2/NO ~~$>$~~ $>$ 15) associated with low NO concentrations (NO $<$ 0.2 ppb), which suggests transported pollutants.

In order to identify periods of high CO associated with low NO_x concentrations, we have computed the CO~~/NO_x~~ $/NO_x$ ratio (Figure 5-bottom). When a BB layer reaches the ~~Guinean coast~~Guinea Coast, gaseous nitrogen oxide concentrations are lower than 0.1 ppb (Capes et al., 2009; Reeves et al., 2010), because gaseous nitrogen oxides have been converted into the particulate phase during the transport over the Southeast Atlantic. We therefore expect an increase of CO and constant NO_x,

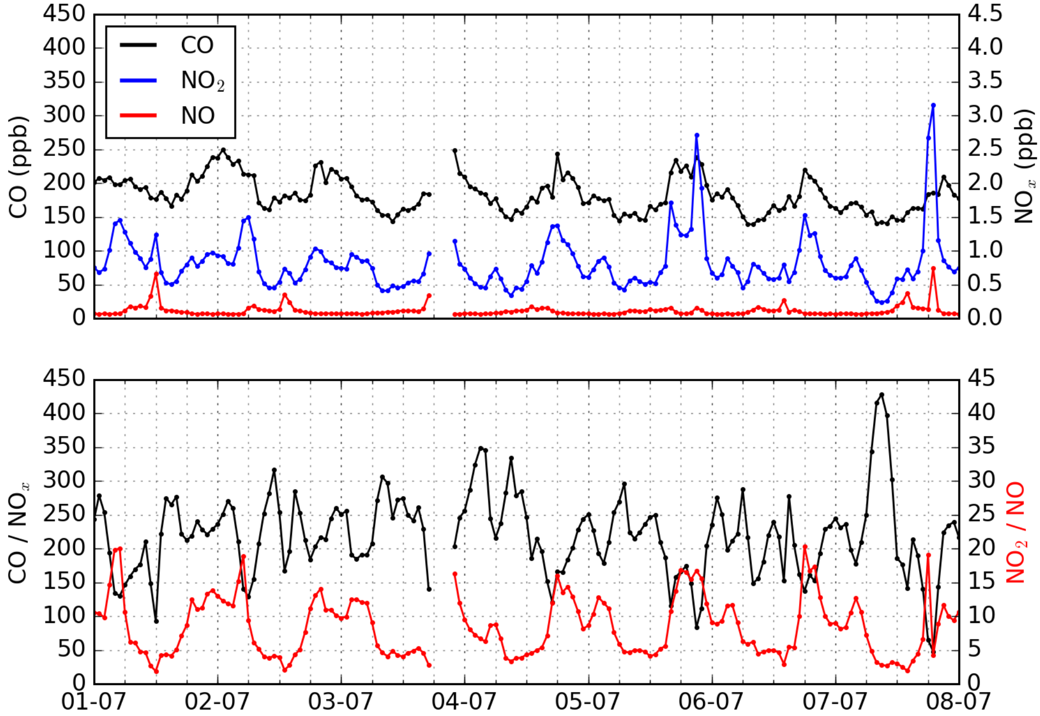

Figure 5. *Time series of (top) carbon monoxide (CO), nitrogen dioxide (NO_2) and nitrogen monoxide (NO) hourly concentration averages (in ppb) observed at Savè (Benin) for the period ~~1–7~~ 1–7 July 2016, and (bottom) of the ratios: CO/~~NO_x~~ /NO_x (in black) and NO/~~NO_2~~ /NO_2 (in red). The vertical dashed lines indicate periods of 6 hours starting at 00:00 UTC.*

when the BB layer reaches Savè without being mixed with URB (containing NO_x in the gaseous phase). At Savè, the CO/~~NO_x~~ /NO_x ratio is not higher after the arrival of the BB layer on 5 July (*cf.* Section 3.1). ~~This result suggests that either~~ There is an increase of CO together with a NO_x increase, thus when the BB layer ~~does not reach Savèin the surface layer or that the BB layer is mostly~~ reaches Savè, it is mixed with urban pollution or transported above the PBL. ~~In order to determine the diurnal cycle of the three pollutants, we present observed hourly averages over 1-7 July together with the maximum and minimum of each hour measured (Figure 6).~~

In order to determine the diurnal cycle of the three pollutants, we present observed hourly averages over 1–7 July together with the maximum and minimum of each hour measured (Figure 6).There is a clear diurnal cycle of hourly CO concentration averages with the minimum occurring at 08:00 UTC (about 160 ppb) and with the maximum occurring between 18:00 and 22:00 UTC (greater than 200 ppb) over the period ~~1–7~~ 1–7 July (Figure 6) and also over the entire campaign period (Figure AA5). This time is in agreement with Adler et al. (2017) and Deetz et al. (2018) who have found using the super-site instrumentation

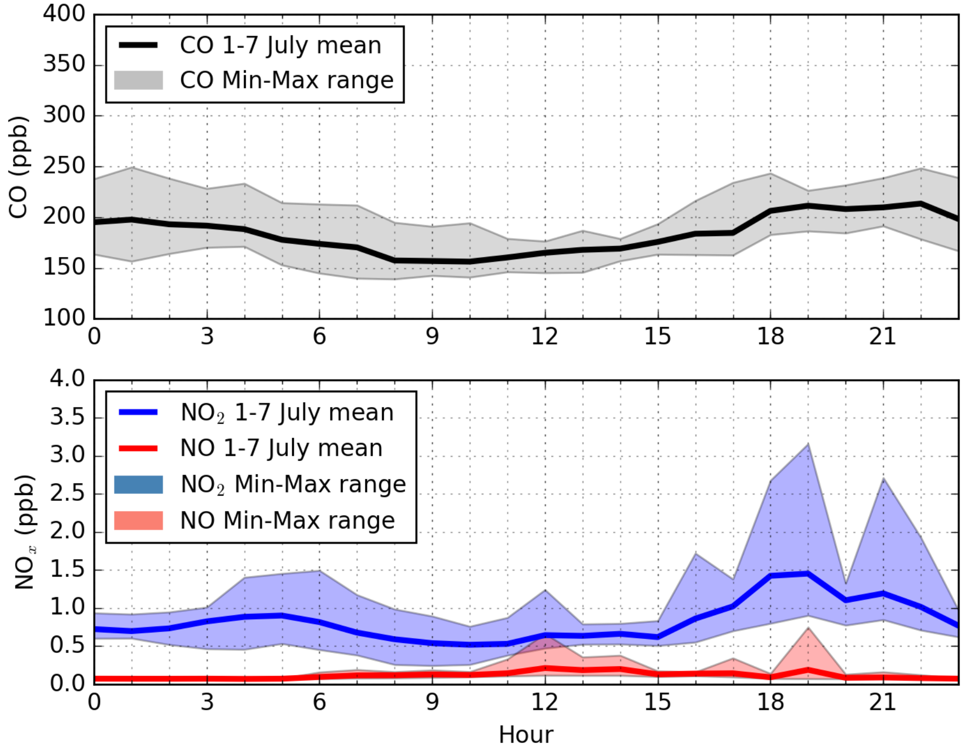

Figure 6. *Hourly diurnal cycles of (top) carbon monoxide (CO in black) and (bottom) nitrogen dioxide (NO_2 in blue) and nitrogen monoxide (NO in red) concentrations (in ppb) observed at Savè (Benin). Means of each hour are presented by the lines over the period 1-7 July 2016 and the upper and lower shading limits correspond to the hourly ranges (maximum and minimum of each hour over the period).*

that the coastal front starts moving northward after 16:00 UTC, reaching Savè in the evening. It also corresponds to the highest hourly minimum (190 ppb) and maximum (250 ppb). It is worth noting that CO concentration remains greater than 180 ppb from 22:00 to 04:00 UTC.

For NO_2, we also note a clear diurnal cycle with low hourly concentration averages between 08:00 and 15:00 UTC, and with high hourly concentration averages (greater than 1 ppb) from 18:00 to 21:00 UTC over the studied period and also over the entire campaign period (Figure AA5). The NO peak at two small NO increases (from 0.2 to 0.6 ppb) at 12:00 and 19:00 UTC is are consistent with the usual time of local activities such as traffic and charcoal cook stoves. At 21:00 UTC, there is a high NO_2 concentration, as well as a high CO concentration, which is not associated with a high NO concentration, suggesting pollution transport because it is the time of the coastal front passage (Adler et al., 2017; Deetz et al., 2018).

The NO_2 diurnal cycle is similar to the one of CO with a minimum at 08:00 UTC (about 0.6 ppb) and a maximum between 18:00 and 21:00 UTC. The main difference of the NO_2 and CO diurnal cycles occurs at night between 21:00 and 02:00 UTC because CO remains high ($\approx$ 200 ppb), whereas NO_2 decreases from 1.3 to 0.7 ppb. This result could be linked to a higher ratio of BB compared to URB.

In conclusion, at Savè, there are similar diurnal cycles of CO and NO_2 with maxima between 18:00 and 21:00 UTC. Moreover NO concentration is very low at 21:00 UTC, indicating pollution transport from the coastal urban agglomerations and not local production. The BB layer could interact with the URB plumes in the PBL, thus increasing the CO concentration. We need to understand how the BB layer is mixed with URB at the coast, and how it is transported further inland.

4.2 Contribution of major coastal cities to the pollution budget at Savè

This section aims at identifying which major cities have a significant contribution to inland pollution at Savè. For this, we analyze the Tracer Experiment 1 described in the models section (*cf.* Table 3).

In order to present this experiment, the synoptic wind patterns and the pollution plumes of the coastal cities with the URB tracers are displayed on a single figure ~~. The~~ (Figure 7). This figure represents an average of the modeled plumes over the period ~~1–7~~ 1–7 July in the monsoon layer (from surface to 1 km). Results are presented in an arbitrary unit with the same isocontour value (Iso1) of tracer concentration for each city (color shadings in Figure 7).

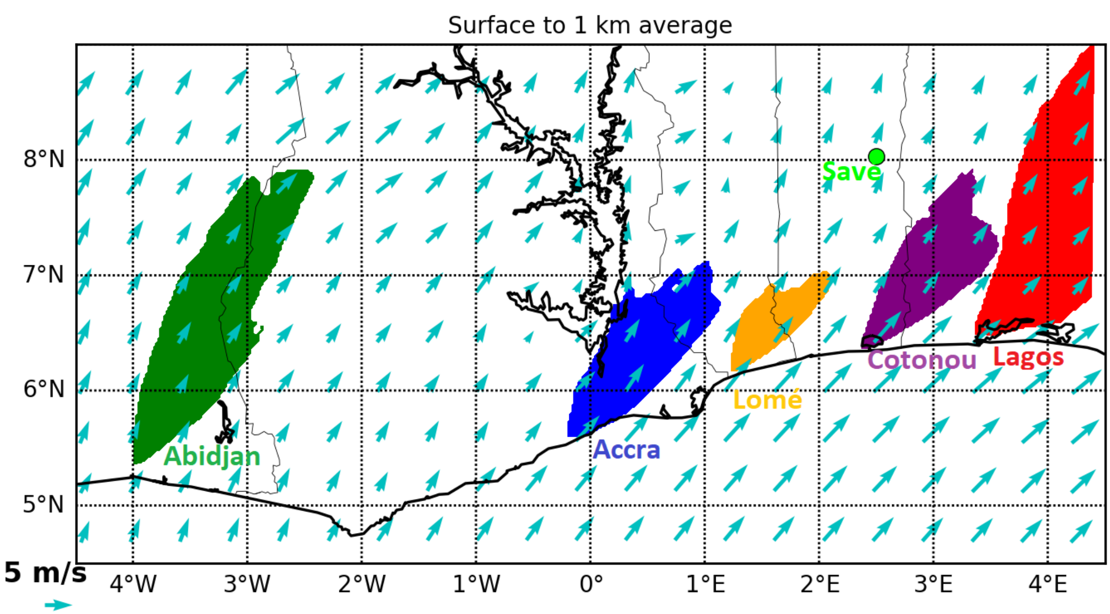

Figure 7. *Maps of URB tracer concentration (in arbitrary unit) averaged over the period 1 to 7 July 2016 in the monsoon layer (from the surface to 1 km amsl). Tracers are released from Abidjan (Ivory Coast) in green, from Accra (Ghana) in blue, from Lomé (Togo) in orange, from Cotonou (Benin) in violet, from Lagos (Nigeria) in red. The same threshold of tracer concentration is used for all city plumes for the color shading (Iso1). Wind vectors at 10 m modeled by WRF are presented by the light blue arrows. The location of the DACCIWA super-site (Savè in Benin) is presented by the light green dot.*

Over the Gulf of Guinea, we can see ~~a stronger northwestward component of the wind with~~ markedly higher wind speed than over the continent. This figure shows that the pollution plumes of Accra, Lomé and Cotonou could reach Savè, while the direction of the Lagos and Abidjan plumes is not oriented towards Savè.

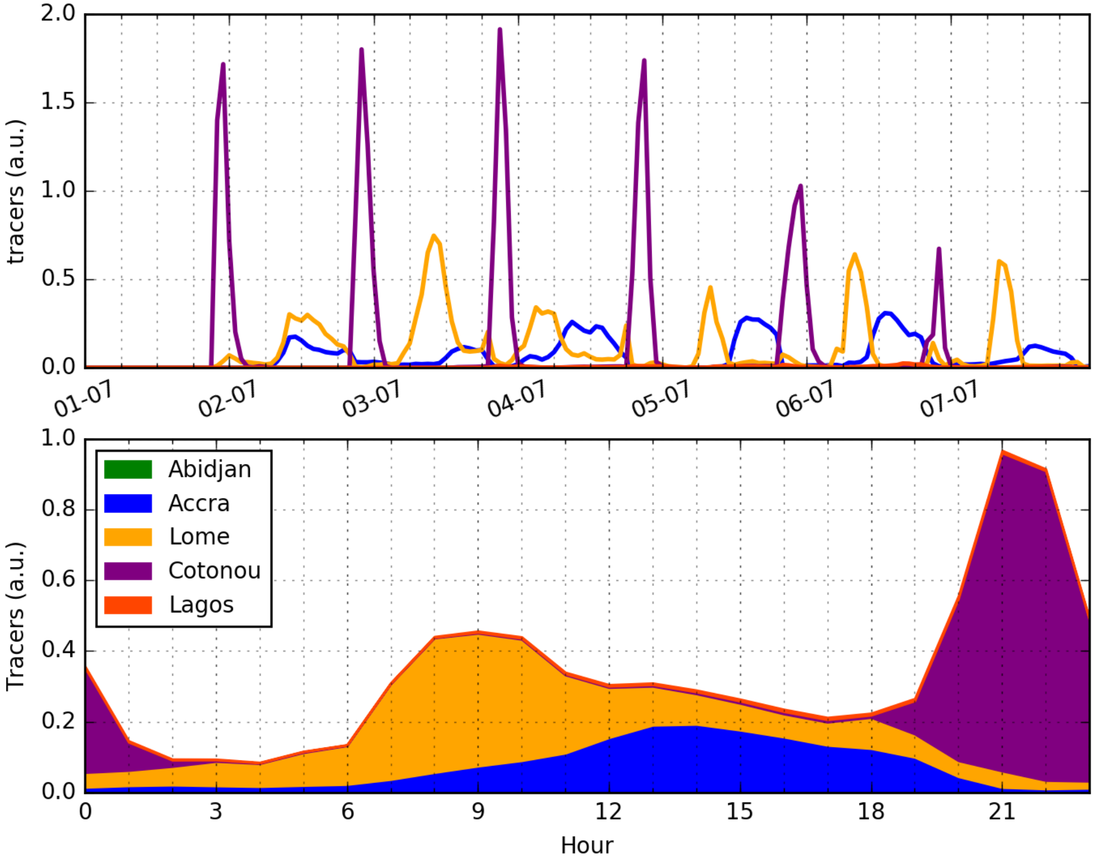

Figure 8. *Time series of hourly URB tracer concentrations (in arbitrary unit) modeled by the CHIMERE model at the DACCIWA field campaign ground station in Savè (Benin) for the period ~~1-7~~ 1–7 July 2016. Urban tracers are released from five coastal cities: Abidjan (Ivory Coast) in green, Accra (Ghana) in blue, Lome (Togo) in orange, Cotonou (Benin) in violet, and Lagos (Nigeria) in red.*

We now focus on the temporal variability reproduced by the tracer experiment at Savè (light green dot in Figure 7). The tracer concentration of the five cities has been interpolated to Savè coordinates (Figure 8-top). The tracer emissions started on 1 July at 00:00 UTC. The first tracer plume that reaches Savè ~~typically~~ is that from Cotonou in the evening. We can see that tracers emitted from Cotonou reach Savè every day in the evening, typically at around 19:00 UTC~~is from Cotonou~~. In the morning, the Lomé pollution plume reaches Savè, while the Accra pollution plume reaches Savè in the afternoon. There is a short period when hourly concentrations are at a maximum every day, and this peak is associated with the arrival of the Cotonou plume in the evening. This pattern is seen repeatedly over the entire ~~1–7~~ 1–7 July period. The model clearly predicts identified periods when Savè is under the influence of different cities, which implies that these periods correspond to pollution plumes characterized by different chemical ages.

From 5 to 6 July, the contribution of Cotonou decreases and the Accra and Lomé contributions increase, which suggests a modification of wind patterns. It is worthy of note that Lagos tracers do not reach Savè, although emissions from Lagos are greater than from the other cities. From midnight to the end of the night, there is no city plume reaching Savè. However, we have seen in Section 4.1 that a high CO concentration persists during the night.

The average diurnal cycle of tracers is presented with the contribution of each city (Figure 8-bottom). It confirms that there are distinct periods when Savè is under the successive influences of Lomé in the morning (06:00 to 12:00 UTC), of Accra in the afternoon (12:00 to 18:00 UTC), and of Cotonou in the evening (18:00 to 01:00 UTC). Lagos tracers do not reach Savè because of the southwesterly monsoon flow.

The observed increases in surface concentration may be explained by several processes: long-range transport of the URB plume and/or a local collapse of the nocturnal boundary layer, quickly concentrating locally emitted pollutants. In our case, the dominant effect is the long-range transport, which is mainly associated with the transport of the Cotonou plume. Moreover, during the entire campaign, we did not note any increase of NO at night (Figure AA4 and Figure AA5). These results suggest that the Cotonou plume is affecting Savè during a short period with a maximum between 21:00 and 22:00 UTC (about 2 times greater than the peak magnitude due to Lomé). This is in agreement with observations of CO and NO_x concentrations (*cf.* Section 4.1). We now need to investigate the diurnal cycle of pollutant transport from coastal cities.

4.3 Mixing and transport of urban anthropogenic and biomass burning

In this section, results of Tracer Experiment 2 (*cf.* Table 3) are discussed. We present the spatial patterns of URB and BB tracer concentrations averaged over the three layers described in Section 3.2 and then we analyze the vertical structure of these two types of pollution. We focus on 5 July when the BB layer reaches the Guinea Coast (*cf.* Section3.1). The first layer height is 300 m, which is roughly the minimum PBL top height at night.

In order to analyze the interactions between URB emissions and the BB layer, we reproduce the BB layer use the information on the spatial characteristics and vertical extent of BB the layer derived from MODIS and CALIPSO observations (Section 3.1) by releasing passive gaseous tracers from 5 July at 00:00 UTC to 6 July at 23:00 UTC with a spatial horizontal extent from 1°W to 2°E at 4.5°N , and the altitude as suggested by satellite observations (Figure A2) at and with an altitude of ≈ 1.5 km amsl from 5 July at 00:00 UTC to 6 July at 23:00 UTC (*cf.* Section 4.2Table 3). Although a non-negligible part of BB is transported in the marine PBL, measurements performed during the DACCIWA campaign have confirmed that the BB layer altitude over the ocean is mostly between 1 and 3 km amsl (Haslett et al. , in preparation). (Reeves et al., 2010). URB tracers are not separated by city in this experiment. The threshold of URB tracer concentration for the isocontour presented on the maps is Iso2 = Iso1 × 5 (Figure 9).

On 5 July at 13:00 UTC when shallow dry convection is well developed and looking at the URB in the surface layer, the Accra and Abidjan plumes are transported towards the north, whereas the Lomé, Cotonou and Lagos plumes have a strong eastward component (Figure 9-top-left). This matches the difference in wind direction along the coastline. From 1 to 2 km

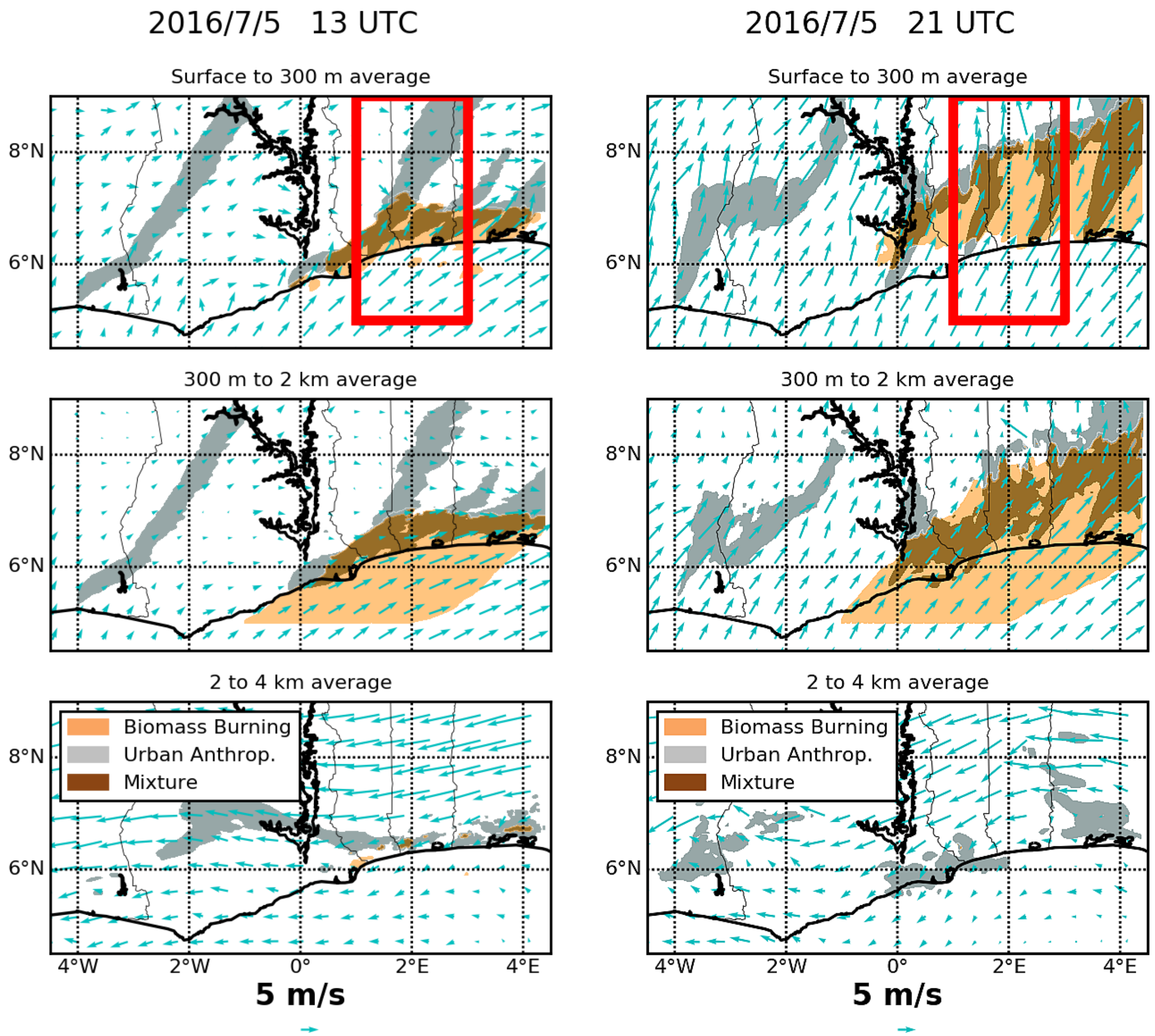

Figure 9. *Maps of concentrations of URB (in gray) and BB (in brown) numerical tracers on 5 July 2016 at 13:00 UTC (left) and at 21:00 UTC (right). Concentrations are averaged over three layers (top) from the surface to 300 m amsl, (middle) from 0.3 to 2 km amsl, (bottom) from 2 to 4 km amsl. Wind vectors at 10 m from the WRF model are presented by the light blue arrows. The meridional-vertical transect shown in Figure 10 corresponds to the zonally averaged area of the red rectangle.*

amsl, the URB tracer distribution is almost the same (with lower wind speed), which shows that the PBL is reaching 1 km amsl at 13:00 UTC. The BB layer emitted at 4.5°N is transported northward between 1 and 2 km amsl over the Gulf of Guinea. BB tracers are not mixed with the marine PBL but with URB tracers from the coast to ≈ 7°N.

On 5 July at 21:00 UTC, when the dry convection has stopped, the model predicts consistent wind speed between the ocean and the continent with a stronger northward component than at 13:00 UTC, especially over the continent. The shape of URB

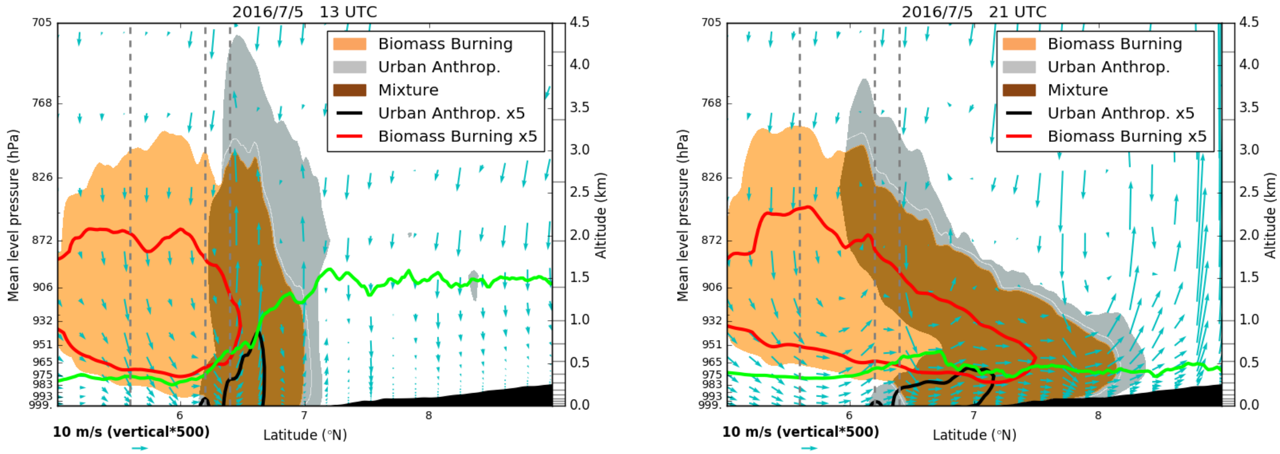

Figure 10. *Meridional-vertical transect of concentrations of URB (in gray) and BB (in brown) numerical tracers on 5 July 2016 at 13:00 UTC (left) and at 21:00 UTC (right). PBL top height from the WRF model is the green line. The vertical dashed gray lines show the latitude of Accra (5.6°N), Lomé (6.2°N) and Cotonou (6.4°N). The black area is the topography. Vectors (light blue arrows) represent wind in the plan of the transect (with an aspect ratio of 500 between the meridional and vertical lengths).*

plumes in the first two layers presents two distinct parts, which seems to follow the change of the wind patterns. The area where BB and URB tracers are mixed extends from the coast to ≈ 8°N.

The vertical structure of the wind is now analyzed using cross-sections along a meridional transect from 1°E to 3°E (the red square in Figure 9). We present the same hours of the simulation (13:00 UTC and 21:00 UTC on 5 July), with isocontours Iso2, and other isocontours (Iso3) for both tracers in order to see the core of the plumes: Iso3 = Iso2 × 5.

The vertical structure changes markedly from 13:00 and 21:00 UTC (Figure 10). At 13:00 UTC, shallow dry convection occurs between the coast and ≈ 7°N, which leads to a vertical mixing of BB and URB tracers (Figure 10). The rising motion at the coast is linked to the coastal front that occurs during the day (Adler et al., 2017; Deetz et al., 2018). The sinking motion over the ocean is linked to the land-sea breeze circulation (Knippertz et al., 2017). BB tracers are transported over the marine PBL without mixing. They reach the surface between the coast and ≈ 7°N. URB and BB tracers accumulate along the coastline until the coastal front begins moving northward, which is in agreement with Adler et al. (2017) and Deetz et al. (2018).

At 21:00 UTC, the NLLJ is established at about 400 m amsl from the coast up to 9°N where the front is located. At the coast itself, the front is not present, thus URB and BB tracers are not mixed anymore. The mixture of URB and BB occurring during the daytime is transported northward up to 8°N. The Iso3 isocontour of BB does not reach the surface. It shows that at night the BB layer penetrates further inland. BB and URB plumes are mostly transported above (between 0.5 and 2.5 km amsl) and within the PBL, respectively.

The discussion in this section is supported by two video supplements (*Click on the links below*):

1) three layer maps https://drive.google.com/open?id=1u5DOyUoaKaimcgoqbbfQl8q5OTtGtujy

2) vertical-meridional transects https://drive.google.com/open?id=1bcwFYld1KS2-b3AgQBdgzh8xo34nC9Ol

The two videos further illustrate the analysis made at 13:00 and 21:00 UTC on 5 July. They also provide useful additional information to analyze the day to night transition leading to the evening maximum at Savè (Section 4.1). Our simulation reproduces the main features of the diurnal cycle, which are that vertical mixing occurs during daytime, while meridional advection of pollutants is most efficient at night (Parker et al., 2005).

~~The~~ From the wind patterns, we note that the coastal front is present from ~~11~~09:00 to ~~16~~15:00 UTC from the coast up to ≈ 7°N. ~~At the same time,~~ It leads to the accumulation of URB pollutants. This period is referred as 'Daytime drying' by Deetz et al. (2018). From 16:00 to 02:00 UTC (*respectively* from 03:00 to 08:00 UTC), the meridional wind increases (resp. decreases) in the PBL and URB pollutants are mostly transported northward within the PBL. This period is referred to 'Atlantic inflow' (*resp.* 'Moist morning') by Deetz et al. (2018).

During the 'Daytime drying' period, we notice that URB and BB tracers accumulate along the coastline in the PBL (on 5 and 6 July from 11:00 to 15:00 UTC). When dry convection stops (at 16:00 UTC), wind speed quickly increases with a stronger northward component. BB and URB tracers are simultaneously transported northward from the coast. From 16:00 to ~~22~~02:00 UTC, the front moves towards the north, and the mixture of BB and URB tracers is advected accordingly. A similar diurnal evolution of BB and URB transport is simulated on 5 and 6 July.

The timing of the coastal front propagation in our simulation is in agreement with Adler et al. (2017) and Deetz et al. (2018), who have shown the same regular occurrence of a coastal front that develops during daytime and propagates inland in the evening. After the frontal passage, there is the establishment of the NLLJ (with a jet axis around 250 m amsl), which is also reproduced in our simulation (with an over-estimation of jet axis altitude of about 150 m).

5 Conclusions

In this study, several observational datasets together with high-resolution model simulation are used to analyze the diurnal cycle of atmospheric pollution transport over SWA. We focus on two distinct pollution sources, urban anthropogenic and biomass burning pollutants (URB and BB respectively), in order to understand their mixing and their advection inland.

We first studied the dynamics and thermodynamics in the ~~lower~~ lowermost troposphere over SWA using aircraft, radio-sounding and ground-based measurements made during part of the DACCIWA field campaign (from 1 to 7 July 2016). ~~In the lowermost troposphere (from the surface to 4 km amsl), the vertical structure of the wind is composed of three layers: (i) from the surface to the PBL top, the wind transports pollutants towards the northeast with an average speed of ≈ 5 m.s^{-1}; (ii) from the PBL top height to 2 km amsl, there is a directional shear layer with low wind speed (< 4 m.s^{-1}); (iii) from 2 to 4 km amsl, there is the AEJ layer with high speed of ≈ 8 m.s^{-1}. The three layers are in good agreement with the WRF meteorological simulations at 2-km resolution. Nevertheless, there is a positive bias of wind speed from the surface to 2 km amsl~~

~~and the modeled PBL height is generally over-estimated, which could affect the dilution of urban plumes, but consequences on pollution transport should be limited to the relative intensity of the different plumes.~~

The second part of the study uses high-resolution numerical tracer experiments. We analyzed pollution transport from the main urban emission centres of the ~~Guinean coast~~ Guinea Coast (Abidjan, Accra, Lomé, Cotonou and Lagos) ~~.~~ at the super-site of Savè in order to assess the impact on the air quality of remote inland cities characterized by low local emissions.

Observations at Savè (185 km to the north of Cotonou) show that there is a clear diurnal cycle of NO_2 and CO, with a maximum occurring every day between 18:00 and 22:00 UTC, suggesting URB transport from remote emission sites. From the tracer experiments, we demonstrated that there are clear and successive periods of the day when air quality in Savè is affected by different city plumes. Precisely, the contribution of tracers released from Lomé is greater than 50 % (of the total amount of tracers) between 02:00 to 12:00 UTC, while from 12:00 to 18:00 UTC tracers released from Accra constitute the main contributor. Then, during 3 hours (from 20:00 to 22:00 UTC), tracers released from Cotonou reach Savè leading to a contribution greater than 80 %, while it is lower than 10 % during the other 15 hours (from 03:00 to 18:00 UTC). Over the period, tracers released from Cotonou represent a contribution of 40 %, from Lomé of 36 % and from Accra of 23 %. Our results suggest that the successive periods affected by different city plumes are characterized by different chemical ages.

~~To assess the impact of BB on the air quality in Savè, we added a BB layer in the tracer experiments based on satellite observations from MODIS ad CALIOP. The experiment suggest that URB and BB (transported from Central Africa) are mixed along the coastline during the day, whereas at night, URB plumes are transported within the shallow PBL (below about 300 m amsl) and the BB layer is mostly transported between the PBL top and 2 km amsl. The mixture of both URB and BB accumulated over coastal areas is transported northward in the surface layer from 16:00 UTC onward and reaches Savè (185 km to the north) at 21:00 UTC.~~ Previous studies have already highlighted the importance of the diurnal cycle of the wind along the coastline in the lowermost troposphere over the Gulf of Guinea during the monsoon (Parker et al., 2005; Lothon et al., 2008; Schrage and Fink, 2012; Schuster et al., 2013; Adler et al., 2017; Deetz et al., 2018), and suggested an influence on pollution transport. ~~Our results shows that the coastal front is associated with URB and BB accumulation from 11:00 to 16:00 UTC, and its northward moving is associated with the mixture transport of both pollutants, reaching 8°N at 21:00 UTC.~~

The WRF simulation reproduces a diurnal cycle of the wind over SWA in agreement with Adler et al. (2017) and Deetz et al. (2018). Indeed, the structure of the wind changes from the morning to the evening. When the shallow dry convection over the land is well developed, wind speed in the PBL reaches a minimum. A coastal front develops during the day (from 09:00 to 15:00 UTC) and when it ceases, wind speed quickly increases with a stronger northward component. ~~At night, most of the coastal URB~~ There is a specific time of the day (16:00 to 02:00 UTC) for the transport of pollutants from the coast toward the north, which affects inland air quality over SWA, human health as well as radiative transfer and the diurnal cycle of low-level clouds.

Our results based on modeling experiments suggest that URB and BB (transported from Central Africa) are accumulated and mixed along the coastline during the day from 09:00 to 16:00 UTC, whereas at night, URB plumes are transported within the ~~planetary boundary layer~~ shallow PBL (below about ~~500 m above sea level), whereas the BB are mostly transported above it. Our results suggest that BB are generally mixed with urban pollutants emitted along the coastline when it impacts inland~~

ground level air quality300 m amsl) and the BB layer is mostly transported between the PBL top and 2 km amsl. The mixture of both URB and BB accumulated over coastal areas is transported northward in the surface layer from 16:00 UTC onward and reaches Savè at 21:00 UTC.

Over SWA, both wind and URB emissions have a diurnal cycle. The strength of numerical tracer experiments is to enable the dichotomy between the variability linked to the meteorology and the emissions by imposing a constant emission (*i.e.* we do not account for any diurnal cycle). In this article, only the observed variability linked to the meteorology is analyzed, we demonstrated that they are clear periods of the day when Savè is impacted by pollution plumes from different cities. In future research, integrated analyses should be conducted to characterize both the URB plumes and the BB layer in terms of composition, gaseous and particulate phase, oxidation of the organic components, and spatio-temporal variability. The DACCIWA campaign provides unique and valuable observations that will allow the investigation of the perspectives opened by this article based on tracer experiments.

Acknowledgements. The research leading to these results has received funding from the European Union 7th Framework Programme (FP7/2007-2013) under Grant Agreement no. 603502 (EU project DACCIWA: Dynamics-aerosol-chemistry-cloud interactions in West Africa). The Service des Avions Français Instrumentés pour la Recherche en Environnement (SAFIRE, a joint entity of CNRS, Météo-France and CNES and operator of the ATR 42), the British Antarctic Survey (BAS, operator of the Twin Otter) and the Deutsches Zentrum für Luft- und Raumfahrt (operator of the Falcon 20) are thanked for their support. We acknowledge Claire Delon and Fabienne Lohou (Laboratoire d'Aérologie) for helpful discussions.

References

Adler, B., Kalthoff, N., and Gantner, L.: Nocturnal low-level clouds over southern West Africa analysed using high-resolution simulations, Atmospheric Chemistry and Physics, 17, 899–910, https://doi.org/10.5194/acp-17-899-2017, 2017.

Andela, N. and Van Der Werf, G. R.: Recent trends in African fires driven by cropland expansion and El Niño to la Niña transition, Nature Climate Change, 4, 791–795, https://doi.org/10.1038/nclimate2313, 2014.

Brito, J., Freney, E., Dominutti, P., Borbon, A., Haslett, S. L., Colomb, A., Dupuy, R., Denjean, C., Burnet, F., Bourrianne, T., Deroubaix, A., Sellegri, K., Coe, H., Flamant, C., Knippertz, P., and Schwarzenboeck, A.: Assessing the role of anthropogenic and biogenic sources on PM₁ over Southern West Africa using aircraft measurements, Atmospheric Chemistry and Physics, 18, 757–772, https://doi.org/10.5194/acp-18-757-2018, 2018.

Capes, G., Murphy, J. G., Reeves, C. E., McQuaid, J. B., Hamilton, J. F., Hopkins, J. R., Crosier, J., Williams, P. I., and Coe, H.: Secondary organic aerosol from biogenic VOCs over West Africa during AMMA, Atmospheric Chemistry and Physics, 9, 3841–3850, https://doi.org/10.5194/acp-9-3841-2009, 2009.

Crumeyrolle, S., Tulet, P., Gomes, L., Garcia-Carreras, L., Flamant, C., Parker, D. J., Matsuki, A., Formenti, P., and Schwarzenboeck, A.: Transport of dust particles from the Bodélé region to the monsoon layer - AMMA case study of the 9-14 June 2006 period, Atmospheric Chemistry and Physics, 11, 479–494, https://doi.org/10.5194/acp-11-479-2011, 2011.

Deetz, K., Vogel, H., Haslett, S., Knippertz, P., Coe, H., and Vogel, B.: Aerosol liquid water content in the moist southern West African monsoon layer and its radiative impact, Atmospheric Chemistry and Physics Discussions, pp. 1–44, https://doi.org/10.5194/acp-2018-420, 2018.

Deroubaix, A., Flamant, C., Menut, L., Siour, G., Mailler, S., Turquety, S., Briant, R., Khvorostyanov, D., and Crumeyrolle, S.: Interactions of Atmospheric Gases and Aerosols with the Monsoon Dynamics over the Sudano-Guinean region during AMMA, Atmospheric Chemistry and Physics, 18, 445–465, https://doi.org/10.5194/acp-18-445-2018, 2018.

Derrien, S. and Bezombes, Y.: DACCIWA field campaign, Savè super-site, UPS instrumentation, https://doi.org/10.6096/dacciwa.1618, 2016.

DGSCN report: Quatrième Recensement Général de la Population et de l'Habitation du Togo - RGPH4, Direction Générale de la Statistique et de la Comptabilité Nationale, Ministère de la Planification, du Développement et de l'Aménagement du Territoire, http://www.stat-togo.org/contenu/pdf/pb/pb-vol-2-rgph4-tg-2010.pdf,[Accessed:21/03/2018], 2016.

Djossou, J., Léon, J.-F., Akpo, A. B., Liousse, C., Yoboué, V., Bedou, M., Bodjrenou, M., Chiron, C., Galy-Lacaux, C., Gardrat, E., Abbey, M., Keita, S., Bahino, J., Touré N'Datchoh, E., Ossohou, M., and Awanou, C. N.: Mass concentration, optical depth and carbon composition of particulate matter in the major southern West African cities of Cotonou (Benin) and Abidjan (Côte d'Ivoire), Atmospheric Chemistry and Physics, 18, 6275–6291, https://doi.org/10.5194/acp-18-6275-2018, 2018.

Ek, M. B., Mitchell, K. E., Lin, Y., Rogers, E., Grunmann, P., Koren, V., Gayno, G., and Tarpley, J. D.: Implementation of Noah land surface model advances in the National Centers for Environmental Prediction operational mesoscale Eta model, Journal of Geophysical Research: Atmospheres, 108, n/a–n/a, https://doi.org/10.1029/2002JD003296, 2003.

Fink, A. H., Agustí-Panareda, A., Parker, D. J., Lafore, J.-P., Ngamini, J.-B., Afiesimama, E., Beljaars, A., Bock, O., Christoph, M., Didé, F., Faccani, C., Fourrié, N., Karbou, F., Polcher, J., Mumba, Z., Nuret, M., Pohle, S., Rabier, F., Tompkins, A. M., and Wilson, G.: Operational meteorology in West Africa: observational networks, weather analysis and forecasting, Atmospheric Science Letters, 12, 135–141, https://doi.org/10.1002/asl.324, 2011.

Flamant, C., Lavaysse, C., Todd, M. C., Chaboureau, J. P., and Pelon, J.: Multl-platform observations of a springtime case of Bodele and Sudan dust emission, transport and scavenging over West Africa, Quarterly Journal of the Royal Meteorological Society, 135, 413–430, https://doi.org/10.1002/qj.376, 2009.

Flamant, C., Deroubaix, A., Chazette, P., Brito, J., Gaetani, M., Knippertz, P., Fink, A. H., de Coetlogon, G., Menut, L., Colomb, A., Denjean, C., Meynadier, R., Rosenberg, P., Dupuy, R., Schwarzenboeck, A., and Totems, J.: Aerosol distribution in the northern Gulf of Guinea: local anthropogenic sources, long-range transport and the role of coastal shallow circulations, Atmospheric Chemistry and Physics, 18, 12 363–12 389, https://doi.org/10.5194/acp-18-12363-2018, 2018a.

Flamant, C., Knippertz, P., Fink, A. H., Akpo, A., Brooks, B., Chiu, C. J., Coe, H., Danuor, S., Evans, M., Jegede, O., Kalthoff, N., Konaré, A., Liousse, C., Lohou, F., Mari, C., Schlager, H., Schwarzenboeck, A., Adler, B., Amekudzi, L., Aryee, J., Ayoola, M., Batenburg, A. M., Bessardon, G., Borrmann, S., Brito, J., Bower, K., Burnet, F., Catoire, V., Colomb, A., Denjean, C., Fosu-Amankwah, K., Hill, P. G., Lee, J., Lothon, M., Maranan, M., Marsham, J., Meynadier, R., Ngamini, J.-B., Rosenberg, P., Sauer, D., Smith, V., Stratmann, G., Taylor, J. W., Voigt, C., and Yoboué, V.: The Dynamics-Aerosol-Chemistry-Cloud Interactions in West Africa field campaign: Overview and research highlights, Bulletin of the American Meteorological Society, 99, 83–104, https://doi.org/10.1175/BAMS-D-16-0256.1, 2018b.

Giglio, L., Csiszar, I., and Justice, C. O.: Global distribution and seasonality of active fires as observed with the Terra and Aqua Moderate Resolution Imaging Spectroradiometer (MODIS) sensors, Journal of Geophysical Research: Biogeosciences, 111, 1–12, https://doi.org/10.1029/2005JG000142, 2006.

Hong, S.-Y., Noh, Y., and Dudhia, J.: A new vertical diffusion package with an explicit treatment of entrainment processes., Monthly Weather Review, 134, 2318–2341, https://doi.org/10.1175/MWR3199.1, 2006.

Hsu, N. C., Jeong, M.-J., Bettenhausen, C., Sayer, a. M., Hansell, R., Seftor, C. S., Huang, J., and Tsay, S.-C.: Enhanced Deep Blue aerosol retrieval algorithm: The second generation, Journal of Geophysical Research: Atmospheres, 118, 9296–9315, https://doi.org/10.1002/jgrd.50712, 2013.

INSAE report: Quatrième Recensement Général de la Population et de l'Habitation du Bénin - RGPH4, Institut National de la Statistique et de l'Analyse Economique, Direction des Etudes Démographique, Ministère du Développement, de l'Analyse Economique et de la Prospective, http://www.insae-bj.org/recensement-population.html,[Accessed:21/03/2018], 2015.

Janicot, S., Thorncroft, C. D., Ali, A., Asencio, N., Berry, G., Bock, O., Bourles, B., Caniaux, G., Chauvin, F., Deme, A., Kergoat, L., Lafore, J.-P., Lavaysse, C., Lebel, T., Marticorena, B., Mounier, F., Nedelec, P., Redelsperger, J.-L., Ravegnani, F., Reeves, C. E., Roca, R., de Rosnay, P., Schlager, H., Sultan, B., Tomasini, M., and Ulanovsky, A.: Large-scale overview of the summer monsoon over West Africa during the AMMA field experiment in 2006, https://doi.org/10.5194/angeo-26-2569-2008, 2008.

Kalthoff, N., Lohou, F., Brooks, B., Jegede, G., Adler, B., Babić, K., Dione, C., Ajao, A., Amekudzi, L. K., Aryee, J. N. A., Ayoola, M., Bessardon, G., Danuor, S. K., Handwerker, J., Kohler, M., Lothon, M., Pedruzo-Bagazgoitia, X., Smith, V., Sunmonu, L., Wieser, A., Fink, A. H., and Knippertz, P.: An overview of the diurnal cycle of the atmospheric boundary layer during the West African monsoon season: Results from the 2016 observational campaign, Atmospheric Chemistry and Physics, pp. 2913–2928, https://doi.org/10.5194/acp-2017-631, 2018.

Keita, S., Liousse, C., Yoboué, V., Dominutti, P., Guinot, B., Assamoi, E.-m., Borbon, A., Haslett, S. L., Bouvier, L., Colomb, A., Coe, H., Akpo, A., Adon, J., Bahino, J., Doumbia, M., Djossou, J., Galy-Lacaux, C., Gardrat, E., Gnamien, S., Léon, J. F., Ossohou, D., Touré, E., and Roblou, L.: Particle and VOC emission factor measurements for anthropogenic sources in West Africa, Atmospheric Chemistry and Physics, 18, 7691–7708, https://doi.org/10.5194/acp-18-7691-2018, 2018.

Knippertz, P., Coe, H., Chiu, J. C., Evans, M. J., Fink, A. H., Kalthoff, N., Liousse, C., Mari, C., Allan, R. P., Brooks, B., Danour, S., Flamant, C., Jegede, O. O., Lohou, F., and Marsham, J. H.: The DACCIWA project: Dynamics-aerosol-chemistry-cloud interactions in West Africa, Bulletin of the American Meteorological Society, p. 150203142711003, https://doi.org/10.1175/BAMS-D-14-00108.1, 2015a.

Knippertz, P., Evans, M. J., Field, P. R., Fink, A. H., Liousse, C., and Marsham, J. H.: The possible role of local air pollution in climate change in West Africa, Nature Climate Change, 5, 815–822, https://doi.org/10.1038/nclimate2727, 2015b.

Knippertz, P., Fink, A. H., Deroubaix, A., Morris, E., Tocquer, F., Evans, M. J., Flamant, C., Gaetani, M., Lavaysse, C., Mari, C., Marsham, J. H., Meynadier, R., Affo-Dogo, A., Bahaga, T., Brosse, F., Deetz, K., Guebsi, R., Latifou, I., Maranan, M., Rosenberg, P. D., and Schlueter, A.: A meteorological and chemical overview of the DACCIWA field campaign in West Africa in June–July 2016, Atmospheric Chemistry and Physics, 17, 10 893–10 918, https://doi.org/10.5194/acp-17-10893-2017, 2017.

Kulkarni, S., Sobhani, N., Miller-Schulze, J. P., Shafer, M. M., Schauer, J. J., Solomon, P. A., Saide, P. E., Spak, S. N., Cheng, Y. F., Denier van der Gon, H. A. C., Lu, Z., Streets, D. G., Janssens-Maenhout, G., Wiedinmyer, C., Lantz, J., Artamonova, M., Chen, B., Imashev, S., Sverdlik, L., Deminter, J. T., Adhikary, B., D Allura, A., Wei, C., and Carmichael, G. R.: Source sector and region contributions to BC and PM2.5 in Central Asia, Atmospheric Chemistry and Physics, 15, 1683–1705, https://doi.org/10.5194/acp-15-1683-2015, 2015.

Lafore, J.-P., Flamant, C., Guichard, F., Parker, D. J., Bouniol, D., Fink, a. H., Giraud, V., Gosset, M., Hall, N., Höller, H., Jones, S. C., Protat, a., Roca, R., Roux, F., Saïd, F., and Thorncroft, C.: Progress in understanding of weather systems in West Africa, Atmospheric Science Letters, 12, 7–12, https://doi.org/10.1002/asl.335, 2011.

Lelieveld, J., Evans, J. S., Fnais, M., Giannadaki, D., and Pozzer, A.: The contribution of outdoor air pollution sources to premature mortality on a global scale., Nature, 525, 367–71, https://doi.org/10.1038/nature15371, 2015.

Liousse, C., Keita, S., N'Datchoch Touré, E., Doumbia, T., Yoboué, V., Assamoi, E., Haslett, S., Roblou, L., Léon, J.-F., Galy-Lacaux, C., et al.: African Anthropogenic Emissions Inventories for gases and particles from 1990 to 2016, EGU General Assembly Conference Abstracts, 19, 19 601, 2017.

Lothon, M., Saïd, F., Lohou, F., and Campistron, B.: Observation of the Diurnal Cycle in the Low Troposphere of West Africa, Monthly Weather Review, 136, 3477–3500, https://doi.org/10.1175/2008MWR2427.1, 2008.

Mailler, S., Menut, L., Khvorostyanov, D., Valari, M., Couvidat, F., Siour, G., Turquety, S., Briant, R., Tuccella, P., Bessagnet, B., Colette, A., Létinois, L., and Meleux, F.: CHIMERE-2016: From urban to hemispheric chemistry-transport modeling, Geoscientific Model Development Discussions, 0, 1–41, https://doi.org/10.5194/gmd-2016-196, 2016.

Marais, E., Jacob, D., Wecht, K., Lerot, C., Zhang, L., Yu, K., Kurosu, T., Chance, K., and Sauvage, B.: Anthropogenic emissions in Nigeria and implications for atmospheric ozone pollution: A view from space, Atmospheric Environment, 99, 32–40, https://doi.org/10.1016/j.atmosenv.2014.09.055, 2014.

Marais, E. A. and Wiedinmyer, C.: Air Quality Impact of Diffuse and Inefficient Combustion Emissions in Africa (DICE-Africa), Environmental Science & Technology, 50, 10 739–10 745, https://doi.org/10.1021/acs.est.6b02602, 2016.

Maranan, M., Fink, A. H., and Knippertz, P.: Rainfall types over southern West Africa: Objective identification, climatology and synoptic environment, Quarterly Journal of the Royal Meteorological Society, https://doi.org/10.1002/qj.3345, 2018.

Menut, L., Bessagnet, B., Khvorostyanov, D., Beekmann, M., Blond, N., Colette, a., Coll, I., Curci, G., Foret, G., Hodzic, a., Mailler, S., Meleux, F., Monge, J.-L., Pison, I., Siour, G., Turquety, S., Valari, M., Vautard, R., and Vivanco, M. G.: CHIMERE 2013: a model for regional atmospheric composition modelling, Geoscientific Model Development, 6, 981–1028, https://doi.org/10.5194/gmd-6-981-2013, 2013.

Menut, L., Flamant, C., Turquety, S., Deroubaix, A., Chazette, P., and Meynadier, R.: Impact of biomass burning on pollutants surface concentrations in megacities of the Gulf of Guinea, Atmospheric Chemistry and Physics, 18, https://doi.org/10.5194/acp-18-2687-2018, 2018.

Mlawer, E. J., Taubman, S. J., Brown, P. D., Iacono, M. J., and Clough, S. a.: Radiative transfer for inhomogeneous atmospheres: RRTM, a validated correlated-k model for the longwave, Journal of Geophysical Research, 102, 16 663, https://doi.org/10.1029/97JD00237, 1997.

Monks, P. S., Granier, C., Fuzzi, S., Stohl, A., Williams, M. L., Akimoto, H., Amann, M., Baklanov, A., Baltensperger, U., Bey, I., Blake, N., Blake, R. S., Carslaw, K., Cooper, O. R., Dentener, F., Fowler, D., Fragkou, E., Frost, G. J., Generoso, S., Ginoux, P., Grewe, V., Guenther, A., Hansson, H. C., Henne, S., Hjorth, J., Hofzumahaus, A., Huntrieser, H., Isaksen, I. S. A., Jenkin, M. E., Kaiser, J., Kanakidou, M., Klimont, Z., Kulmala, M., Laj, P., Lawrence, M. G., Lee, J. D., Liousse, C., Maione, M., McFiggans, G., Metzger, A., Mieville, A., Moussiopoulos, N., Orlando, J. J., O'Dowd, C. D., Palmer, P. I., Parrish, D. D., Petzold, A., Platt, U., Pöschl, U., Prévôt, A. S. H., Reeves, C. E., Reimann, S., Rudich, Y., Sellegri, K., Steinbrecher, R., Simpson, D., ten Brink, H., Theloke, J., van der Werf, G. R., Vautard, R., Vestreng, V., Vlachokostas, C., and von Glasow, R.: Atmospheric composition change - global and regional air quality, Atmospheric Environment, 43, 5268–5350, https://doi.org/10.1016/j.atmosenv.2009.08.021, 2009.

Pacifico, F., Delon, C., Jambert, C., Durand, P., Morris, E., Evans, M. J., Lohou, F., Derrien, S., Donnou, V. H. E., Houeto, A. V., Reinares Martinez, I., and Brilouet, P.-E.: Measurements of nitric oxide and ammonia soil fluxes from a wet savanna ecosystem site in West Africa during the DACCIWA field campaign, Atmospheric Chemistry and Physics Discussions, pp. 1–37, https://doi.org/10.5194/acp-2017-1198, 2018.

Parker, D. J., Burton, R. R., Diongue-Niang, A., Ellis, R. J., Felton, M., Taylor, C. M., Thorncroft, C. D., Bessemoulin, P., and Tompkins, a. M.: The diurnal cycle of the West African monsoon circulation, Quarterly Journal of the Royal Meteorological Society, 131, 2839–2860, https://doi.org/10.1256/qj.04.52, 2005.

Parker, D. J., Fink, A., Janicot, S., Ngamini, J.-B., Douglas, M., Afiesimama, E., Agusti-Panareda, A., Beljaars, A., Dide, F., Diedhiou, A., Lebel, T., Polcher, J., Redelsperger, J.-L., Thorncroft, C., and Wilson, G. A.: The Amma Radiosonde Program and its Implications for the Future of Atmospheric Monitoring Over Africa, Bulletin of the American Meteorological Society, 89, 1015–1028, https://doi.org/10.1175/2008BAMS2436.1, 2008.

Redelsperger, J. L., Thorncroft, C. D., Diedhiou, A., Lebel, T., Parker, D. J., and Polcher, J.: The African Monsoon Multidisciplinary Analysis: An International Research Project and Field Campaign, Bulletin of the American Meteorological Society, 87, 1739–1746, 2006.

Reeves, C. E., Formenti, P., Afif, C., Ancellet, G., Attié, J. L., Bechara, J., Borbon, A., Cairo, F., Coe, H., Crumeyrolle, S., Fierli, F., Flamant, C., Gomes, L., Hamburger, T., Jambert, C., Law, K. S., Mari, C., Jones, R. L., Matsuki, A., Mead, M. I., Methven, J., Mills, G. P., Minikin, A., Murphy, J. G., Nielsen, J. K., Oram, D. E., Parker, D. J., Richter, A., Schlager, H., Schwarzenboeck, A., and Thouret, V.: Chemical and aerosol characterisation of the troposphere over West Africa during the monsoon period as part of AMMA, Atmospheric Chemistry and Physics, 10, 7575–7601, https://doi.org/10.5194/acp-10-7575-2010, 2010.

Sauvage, B., Thouret, V., Cammas, J.-P., Gheusi, F., Athier, G., and Nédélec, P.: Tropospheric ozone over Equatorial Africa: regional aspects from the MOZAIC data, Atmospheric Chemistry and Physics, 5, 311–335, https://doi.org/10.5194/acp-5-311-2005, 2005.

Sayer, a. M., Hsu, N. C., Bettenhausen, C., and Jeong, M. J.: Validation and uncertainty estimates for MODIS Collection 6 "deep Blue" aerosol data, Journal of Geophysical Research: Atmospheres, 118, 7864–7872, https://doi.org/10.1002/jgrd.50600, 2013.

Sayer, A. M., Munchak, L. A., Hsu, N. C., Levy, R. C., Bettenhausen, C., and Jeong, M. J.: MODIS Collection 6 aerosol products: Comparison between Aqua's e-Deep Blue, Dark Target, and "merged" data sets, and usage recommendations, Journal of Geophysical Research: Atmospheres, 119, 13,965–13,989, https://doi.org/10.1002/2014JD022453, 2014.

Schrage, J. M. and Fink, A. H.: Nocturnal Continental Low-Level Stratus over Tropical West Africa: Observations and Possible Mechanisms Controlling Its Onset, Monthly Weather Review, 140, 1794–1809, https://doi.org/10.1175/MWR-D-11-00172.1, 2012.

Schuster, R., Fink, A. H., and Knippertz, P.: Formation and Maintenance of Nocturnal Low-Level Stratus over the Southern West African Monsoon Region during AMMA 2006, Journal of the Atmospheric Sciences, 70, 2337–2355, https://doi.org/10.1175/JAS-D-12-0241.1, 2013.

Skamarock, W. C. and Klemp, J. B.: A time-split nonhydrostatic atmospheric model for weather research and forecasting applications, Journal of Computational Physics, 227, 3465–3485, https://doi.org/10.1016/j.jcp.2007.01.037, 2008.

Sobhani, N., Kulkarni, S., and Carmichael, G. R.: Source Sector and Region Contributions to Black Carbon and PM2.5 in the Arctic, Atmospheric Chemistry and Physics Discussions, pp. 1–43, https://doi.org/10.5194/acp-2018-65, 2018.

United Nations report: World urbanization prospects: the 2011 revision, Population Division, Department of Economic and Social Affairs, United Nations Secretariat, http://www.un.org/en/development/desa/population/publications/pdf/urbanization/WUP2011_Report.pdf,[Accessed:11/06/2018], 2011.

van Leer, B.: Towards the ultimate conservative difference scheme. V. A second-order sequel to Godunov's method, Journal of Computational Physics, 32, 101–136, https://doi.org/10.1016/0021-9991(79)90145-1, 1979.

von Storch, H., Langenberg, H., and Feser, F.: A Spectral Nudging Technique for Dynamical Downscaling Purposes, Monthly Weather Review, 128, 3664–3673, https://doi.org/10.1175/1520-0493(2000)128<3664:ASNTFD>2.0.CO;2, 2000.

Winker, D. M., Vaughan, M. A., Omar, A., Hu, Y., Powell, K. A., Liu, Z., Hunt, W. H., and Young, S. A.: Overview of the CALIPSO Mission and CALIOP Data Processing Algorithms, Journal of Atmospheric and Oceanic Technology, 26, 2310–2323, https://doi.org/10.1175/2009JTECHA1281.1, 2009.

Winker, D. M., Tackett, J. L., Getzewich, B. J., Liu, Z., Vaughan, M. A., and Rogers, R. R.: The global 3-D distribution of tropospheric aerosols as characterized by CALIOP, Atmospheric Chemistry and Physics, 13, 3345–3361, https://doi.org/10.5194/acp-13-3345-2013, 2013.

Yang, Y., Wang, H., Smith, S. J., Ma, P.-L., and Rasch, P. J.: Source attribution of black carbon and its direct radiative forcing in China, Atmospheric Chemistry and Physics, 17, 4319–4336, https://doi.org/10.5194/acp-17-4319-2017, 2017.

Zuidema, P., Redemann, J., Haywood, J., Wood, R., Piketh, S., Hipondoka, M., and Formenti, P.: Smoke and Clouds above the Southeast Atlantic: Upcoming Field Campaigns Probe Absorbing Aerosol's Impact on Climate, Bulletin of the American Meteorological Society, 97, 1131–1135, https://doi.org/10.1175/BAMS-D-15-00082.1, 2016.

Appendix A: Supplemental Material

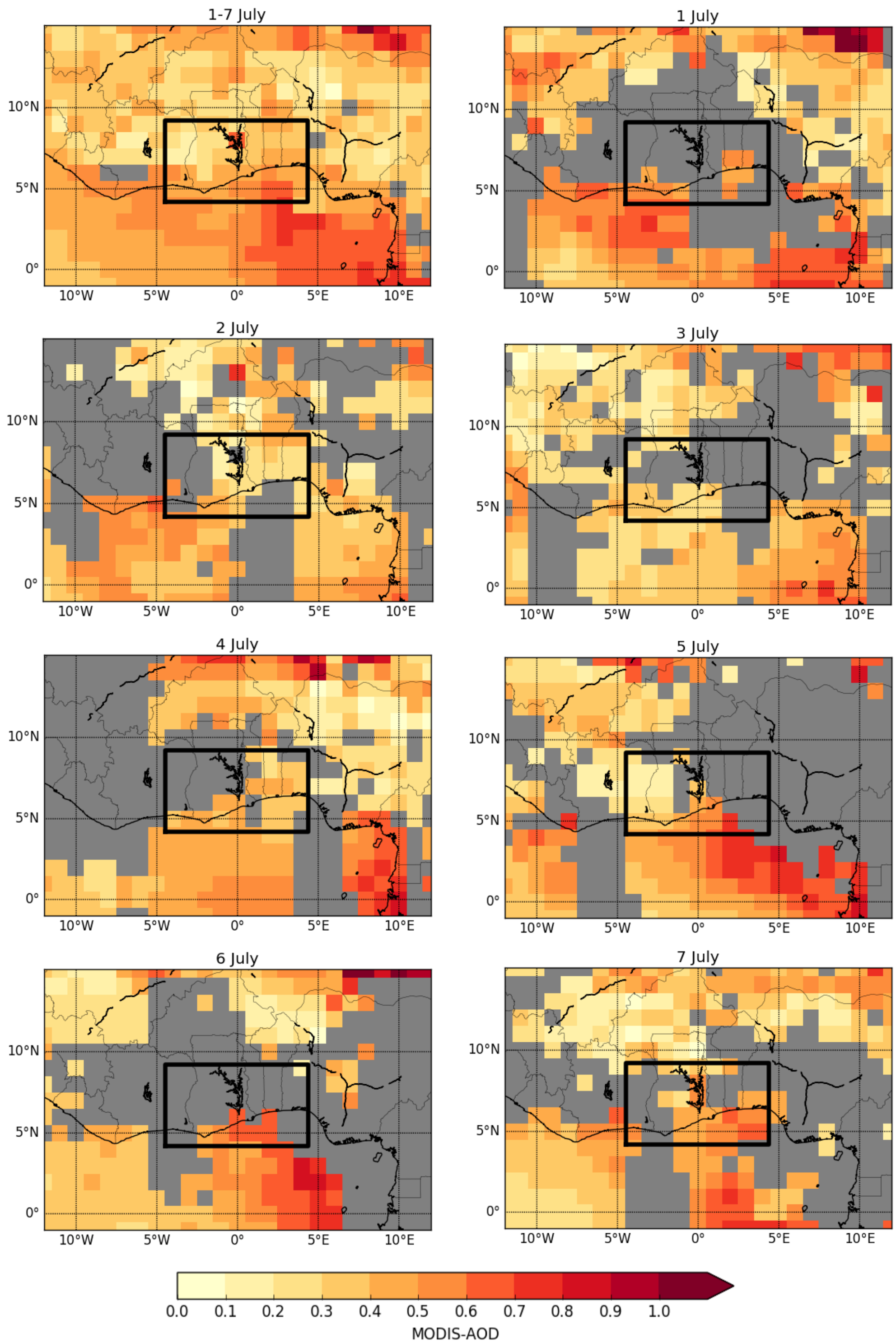

Figure A1. *~~MODIS-AOD~~ MODIS AOD daily average of two products acquired by Aqua and Terra (the combined Dark-Target and Deep-Blue MYD08-D3 and MOD08-D3 products respectively) over the ~~1-7~~ 1–7 July 2016 period (top-left) and over each day of the period. Data excluded by the cloud screening process are in gray. The modeling domain is presented by the black square.*

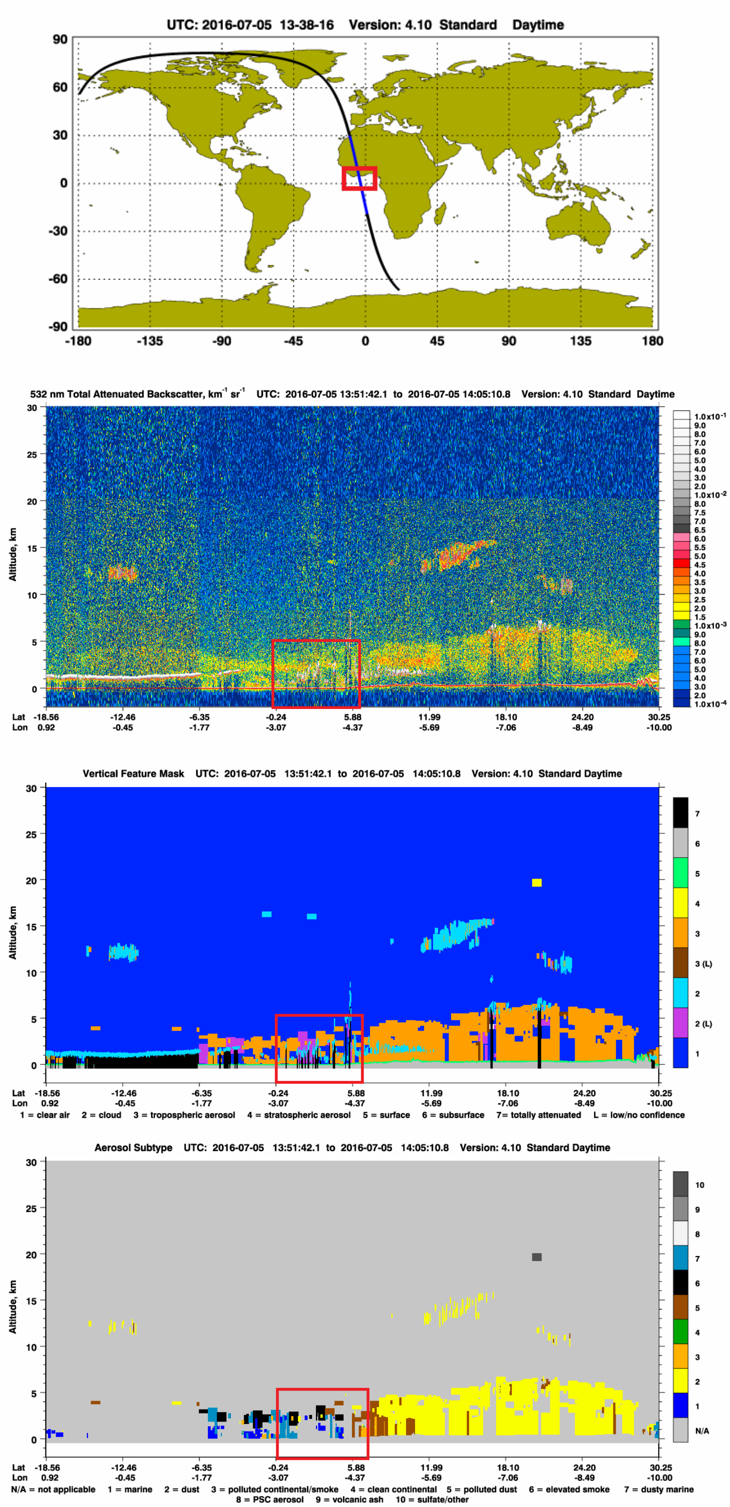

Figure A2. *Space Lidar CALIPSO data onboard the CALIOP platform on 5 July 2016 with the orbit track location, the vertical profile of the total attenuated backscatter, the vertical feature mask and the aerosol subtype. The modeling domain is the red box. (data are available on www-calipso.larc.nasa.gov/products/lidar/browse_images).*

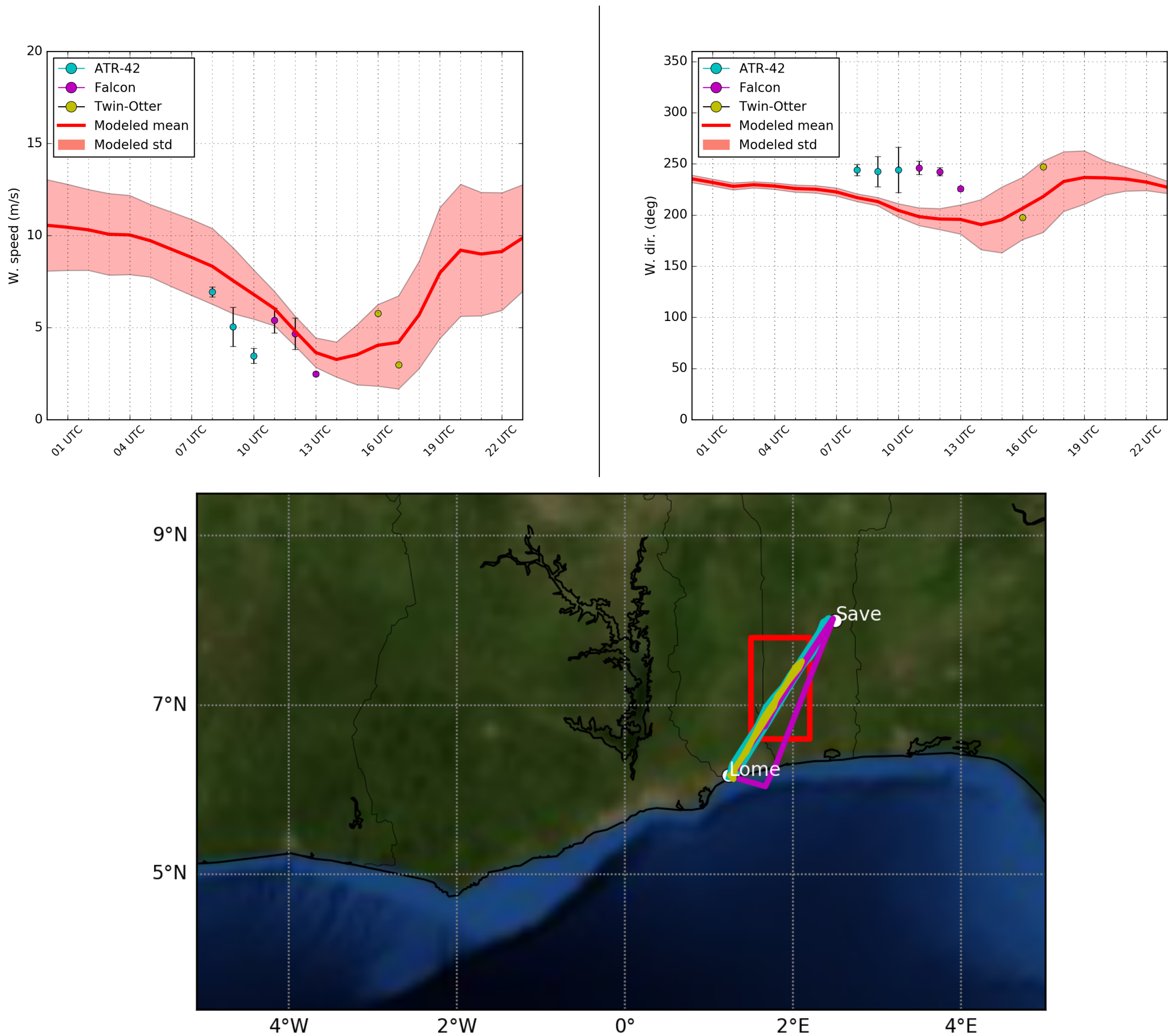

Figure A3. *Wind speed (top-left panel) and direction (top-right panel) hourly averages and standard deviations on 5 July 2016 for all aircraft measurements (dots and errorbars) acquired in a box (latitude from 6.6°N to 7.8°N, in longitudes from 1.5°E to 2.2°E, in altitude from 300 m to 1000 m). The horizontal extent of the box and the aircraft tracks are displayed on the map (bottom panel). Modeled value averages of the whole box are presented by the red line (and standard deviation by red shading). Blue dots correspond to ATR-42 measurements, violet to Falcon and yellow to Twin Otter.*

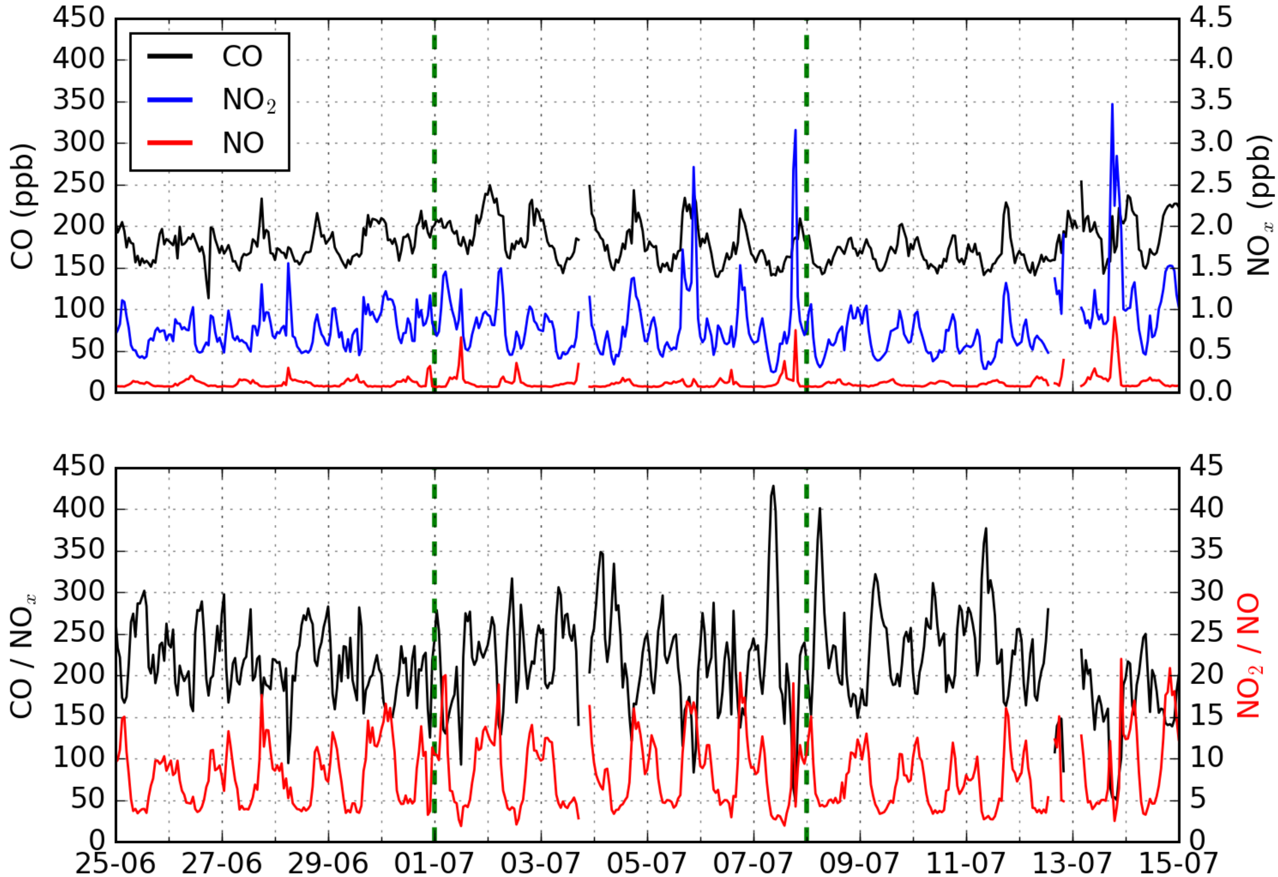

Figure A4. *Time series of (top) carbon monoxide (CO), nitrogen dioxide (NO_2) and nitrogen monoxide (NO) hourly concentrations (in ppb) observed at Savè (Benin) over the entire campaign period (25 June to 15 July 2016), and (bottom) of the ratios: CO/NO_x (in black) and NO_2/NO (in red). The studied period (~~1-7~~ 1–7 July 2016) is defined by the two green dashed vertical lines.*

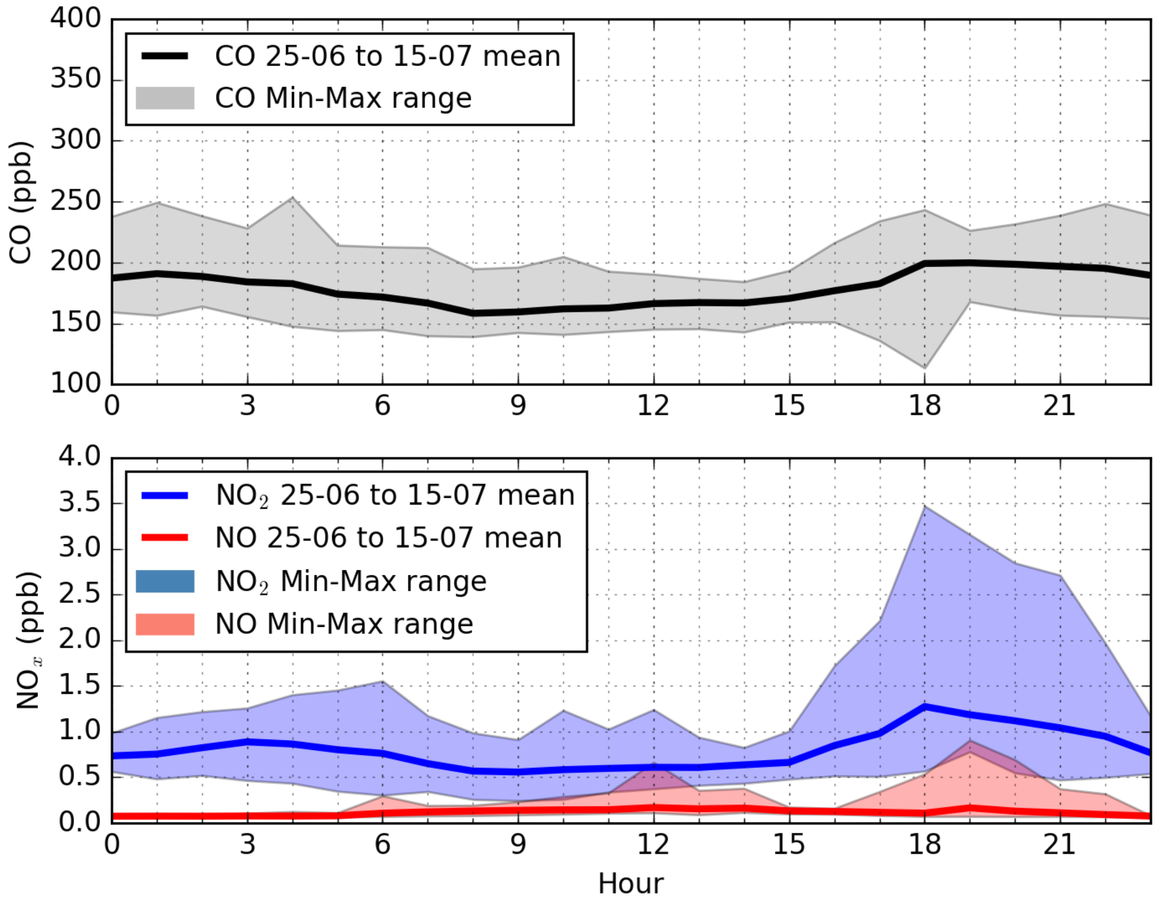

Figure A5. *Hourly diurnal cycles of (top) carbon monoxide (CO in black) and (bottom) nitrogen dioxide (NO_2 in blue) and nitrogen monoxide (NO in red) concentrations (in ppb) observed at Savè (Benin). Means of each hour are presented by the lines over the entire campaign period (25 June to 15 July 2016). The upper and lower shading limits correspond to the hourly ranges (maximum and minimum of each hour over the period).*